Chapter 12
Computational Phantoms for Organ Dose Calculations in Radiation Protection and Imaging

X. George Xu

12.1 Introduction

Dosimetry for ionizing radiation has to do with the determination of amount and distribution pattern of the energy deposited in a part or parts of the human body from internal or external radiation sources. To protect against occupational exposures, dose limits for radiosensitive organs are recommended by international organizations and are adopted as national regulations. In both diagnostic radiology and nuclear medicine, *X*-ray photons and gamma rays traverse through body tissues to form images of the anatomy, depositing radiation energy in organs along the pathway via secondary electrons. Accurate radiation dosimetry is essential but also quite challenging for three reasons: (1) there are many diverse exposure scenarios resulting in unique spatial and temporal relationships between the source and human body; (2) an exposure can involve multiple radiation types, each of which is governed by different radiation physics principles, such as photons (*X*-ray photons, gamma rays, and positrons), electrons, alpha particles, neutrons, and protons; (3) the human body consists of a large number of anatomical structures of diverse shape, composition and density, leading to complex radiation interaction patterns. Since it is inconvenient to place a dosimeter inside the human body, organ dose estimates have been obtained mostly using a physical phantom or a computational phantom that mimics the interior and exterior anatomical features of the human body.

Historically, the term *phantom* was used in most radiological science literature to mean a physical model of the human body. In the radiation protection community, however, the term has also been used to refer to a mathematically defined *anatomical model* that is distinctly different from a physiologically based model such as that related to respiration or blood flow. In this chapter, the phrases, "computational phantom" and "physical phantom," are used to avoid confusion.

X. George Xu (✉)
Nuclear Engineering Program, Rensselaer Polytechnic Institute, Troy, NY, USA
e-mail: xug2@rpi.edu

L. A. DeWerd and M. Kissick (eds.), *The Phantoms of Medical and Health Physics*, Biological and Medical Physics, Biomedical Engineering,
DOI: 10.1007/978-1-4614-8304-5_12,

As discussed extensively in this book, a physical phantom is made of solid materials equivalent to bones and soft tissues that can be molded to resemble the human anatomy and then cut into slices that contain cavities for tiny radiation dosimeters. The approach of using such physical phantoms was known to be expensive and time-consuming due to tedious experimental and radiation safety procedures. Luckily, the advent of the first generation of computers and Monte Carlo simulation methods for nuclear weapons research in the 1940s made it gradually possible to calculate organ doses using a computational phantom. A computational phantom must define the exterior features of the entire human body as well as selected internal organs in terms of volume, mass, and shape. Coupled with information on tissue density and chemical composition, a computational phantom allows for a researcher to use the well-established Monte Carlo methods to calculate radiation interactions and energy deposition in the body [1–3]. Monte Carlo methods, which are based on statistical simulations, have a long history, but the real application to radiation transport simulations and the associated software development arose from nuclear weapons research at Los Alamos National Laboratory during World War II [235]. Although additional work is needed to specify a radiation source and the irradiation geometry, the computational approach has advantageous in comparison with the physical approach in versatility, efficiency, precision, and safety. There are situations, such as internally distributed radiation sources, where the computational approach is the only option. Since the 1960s, the development and application of computational human phantoms became a specialized field of research that intimately associated with radiation protection, imaging, and radiotherapy. Physical phantoms are used to perform benchmark for computational results when needed.

Computational phantoms existed for more than 60 years. The early users were from national laboratories who had access to powerful computers. A focused research group on computational phantoms was not formed until early 1990s when personal computers became a common research tool. Several workshops were held on computational phantoms. In 1996, Dimbylow from National Board of Radiological Protection, UK, organized the first workshop on voxelized computational phantoms [4]. In 2000, Eckerman organized a similar workshop at Oak Ridge National Laboratory, US [244]. By then, there was a widespread interest from the international community about the voxelized computational phantoms. To foster collaboration, I worked with many colleagues to form the Consortium of Computational Human Phantoms (CCHP) in 2005 during the American Nuclear Society Monte Carlo 2005 Topical Meeting in Chattanooga, TN, USA, from April 17–21, 2005 (http://www.virtualphantoms.org). Under the umbrella of CCHP, I later served as the co-editor with Dr. Keith Eckerman, Oak Ridge National Laboratory, for "Handbook of Anatomical Models for Radiation Dosimetry" which was published in 2009 involving 64 authors from 13 countries [245]. In 2011, I organized with Professor Junli Li, the 3rd International Workshop on Computational Phantoms for Radiation Protection, Imaging, and Radiotherapy at Tsinghua University, Beijing, China (http://www.virtualphantoms.org/3rdWorkshopInBeijing.html). The Beijing Workshop was the first time to use this workshop

title and to engage researchers from the non-ionizing radiation dosimetry community. The 4th workshop is being planned for May 20–22, 2013 in Zurich, Switzerland. These workshops have shown to be important in disseminating research ideas, facilitating collaboration, and developing a roadmap for the future.

According to Xu [5], approximately 121 computational phantoms , plus 27 physical phantoms, had been reported in the literature for studies involving ionizing and non-ionizing radiation by the end of 2009. A significant portion of the literature on radiation protection dosimetry is related to the development and application of these phantoms. The organs and body surfaces of computational phantoms have been defined in terms of a variety of solid geometry modeling techniques. Each of these techniques was adopted at specific times in the last 60 years, exhibiting an interesting scientific journey that reflects the advances in computer and medical imaging technologies. Like other research fields, non-technical considerations also had their share in shaping the world of computational phantoms that we know today. As the evolution continues, particularly at the accelerated computing power witnessed in the past decade, it is vitally important to know where we are going. There are many interesting questions facing researchers today. Why did the computational phantoms evolve the way they did? What will be the future directions in this research field? The answers to these questions and many others require an understanding and evaluation of the rationales and processes responsible for some of the most widely used phantoms. The different modeling techniques are defined, and a summary of historical milestones in the development of computational phantoms for ionizing and non-ionizing radiation applications is provided.

12.2 Computational Geometries Used for Phantoms

Computational phantoms are solid geometry models that depict exterior and interior anatomical features of a human body. For radiation dosimetry, a phantom must define the surface of an organ in which radiation interactions and energy depositions are to be calculated by tracing individual particles. Clearly, the construction of such phantoms must consider multiple factors such as anatomy, radiosensitivity, computational efficiency, and geometrical compatibility with a Monte Carlo code.

The computer graphics community has dealt extensively with solid geometry modeling for computer-aided design (CAD). Two general methods of solid geometry modeling have been widely developed: constructive solid geometry (CSG) and boundary representation (BREP) [6–9]. The topology—spatial location and relationship of the surfaces—is fundamentally different for these two methods. CSG allows a modeler to create a solid object using Boolean operators (or the equivalent) to combine very simple objects called primitives. Examples of these primitives include cuboids, cylinders, prisms, pyramids, spheres, cones, and ellipsoids—surfaces that are easily described by quadric equations. CSG

representations are easy to adopt and can yield good results when the objects are relatively simple in shape.

Modern CAD software systems, however, are based on the more powerful BREP methods. There are two types of information in the BREP: topological and geometric. Topological information provides the relationships among vertices, edges, and faces. In addition to connectivity, topological information also includes orientation of edges and faces. In advanced BREP-based CAD, the exterior of an object are defined as NURBS, which afford very smooth surfaces. The faces can alternatively be represented as polygons whose vertices are defined by a set of coordinate values *x*, *y,* and *z*. A polygon mesh or unstructured grid is a collection of vertices and polygons that define the geometric shape of a polyhedral object in CAD. In principle, NURBS and polygonal meshes are interchangeable BREP data structures; however, unlike the CSG representation, BREP is much more flexible because a richer set of operation tools are available (e.g., extrusion, chamfering, blending, drafting, shelling, and tweaking). These features allow BREP-based phantoms to include very complex anatomical features. Furthermore, the BREP technique is ideally suited for surface deformation—an operation necessary for the adjustment of organ size and for organ motion simulations as described later. These surface equations are computationally efficient and are accepted by nearly all Monte Carlo codes. However, even with complicated and carefully designed Boolean operations like this, phantoms based on quadric surfaces are not anatomically realistic in terms of their geometry. When using a Monte Carlo code, the geometry of the left lung is often further simplified by replacing the ellipsoid B with several planes. This type of phantoms is commonly referred to as "stylized" or "mathematical" phantoms.

Voxels, as a CSG modeling technique, define the left lung as an assembly of 3D cuboids. Medical image data can be converted to voxel geometry that provides a direct way to realistically describe the human anatomy. The geometry of a voxel is very simple for existing Monte Carlo codes to handle, although the large number of voxels may require the use of enhanced computer hardware or special Monte Carlo software preparation. On the other hand, each tomographic image slice needs to be treated by a "segmentation " process, which assigns each pixel to an organ or tissue of interest such as the lung, bone, or skin using a unique identification number. It can take a significant amount of time to prepare a voxel-based phantom, because there is no automatic segmentation algorithm that works on all organs. Furthermore, a voxel phantom is based on images for one subject, therefore lacking the anatomical variability associated with organ size, shape, and location that are important in the current paradigm for radiation protection dosimetry. Finally, the boundary of the lung in a voxel phantom is defined by uneven steps instead of a smooth surface. As a result, the anatomical fidelity depends on the voxel size, especially for thin and small tissues such as the skin, eye lens, ribs, and bone marrow. An adjustment to the organ shape will likely involve all underlying voxels, which is computationally inefficient. These types of computational human body models are commonly referred to as "voxel" or "tomographic" phantoms.

An organ can also be defined by the advanced BREP modeling techniques involving NURBS or polygon mesh surfaces. The most common technique to create a BREP-based phantom involves the surface contour extraction of each organ from a tomographic image data set using a commercial software package, followed by the integration of individual organs into a whole-body assembly. In essence, the contours convert the voxels into NURBS or mesh surfaces that are smooth and anatomically realistic. These phantoms are commonly referred to as "NURBS," "mesh," or "BREP" phantoms.

12.3 The Evolution of Computational Phantoms

The historical development of computational phantoms has been reviewed previously, mostly focusing on a certain time period or a particular type of phantoms [10, 11]. These reviews did not explicitly classify phantom modeling techniques, and since the time of their publication, a number of phantoms have been developed using the new BREP methods. Xu [5] was the first to officially group computational phantoms into three generations basing on chronological and technical information in the literature: (1) The first-generation phantoms developed and widely used until 1990s: *stylized* phantoms whose organs are delineated by a combination of simple surface equations, (2) The second-generation phantoms first emerged in late 1980s and then rapidly adopted by many groups in the 1990s: *voxel* or *tomographic* phantoms that are directly based on segmented and labeled medical images of real people, and (3) The third-generation phantoms developed by a relative small group of advanced researchers in the mid-2000s: *BREP* (or mistakenly the *hybrid*) phantoms using B-Splines, NURBS, or polygon meshes.

12.3.1 First-Generation Stylized Phantoms (Prior to the 1990s)

The first-generation computational phantoms were developed for the purpose of assessing organ doses from internally deposited radioactive materials for workers and patients [12, 13–18]. Some of the earliest dose assessment techniques were developed in the first-third of the twentieth century primarily for use with interstitial radiation sources such as radium. With the increase in the size and speed of computers, some progress occurred during the late 1950s and through the 1960s and eventually the efforts led to stylized anthropomorphic phantoms—those resemble the human anatomy.

Stylized phantoms originated from work performed at Oak Ridge National Laboratory (ORNL). The first attempts at developing a computational anthropomorphic phantom were reported by Fisher and Snyder at ORNL in the 1960s [19, 20].

Using CSG modeling techniques involving shapes such as elliptical cylinders and cones, they developed the so-called Fisher-Snyder adult phantom. The adult phantom was assumed to be standing erect with the arms at the sides of the body. Three specific regions were defined; the head and neck, the trunk including the arms, and the legs. The head and neck were represented by a 14 × 20 cm elliptical cylinder with a height of 24 cm. The trunk and arms were modeled as a larger elliptical cylinder, 20 × 40 cm with a height of 70 cm. The legs below the buttocks were modeled as a truncated elliptical cone with a height of 80 cm. Regions of little dosimetric importance were not included, e.g., the hands, feet, ears, and nose. The composition of the phantom was assumed to be tissue distributed homogeneously throughout. No attempt was made to model the lungs or skeleton or to define the locations of specific organs in the phantom. Approximately 120 sub-regions were defined in the phantom, which were used to assign approximate values of the absorbed doses to organs located within specific regions. In some cases, absorbed dose estimates for large organs required the evaluation of the doses deposited in several of these regions. Even though the original phantom was designed for use with internally deposited radionuclides, Snyder saw many other applications. In addition, in 1967, he used the phantom to study the distribution of dose in the body from external, point sources of gamma rays [21]. He studied four photon energies (0.07, 0.15, 0.5, and 1.0 MeV) and four different source locations at distances of one and two meters from the center of the phantom.

Fisher and Snyder also developed the "similitude" children phantoms which were scaled-down versions of the adult with added assumption that the entire body was a homogenous tissue (i.e., the lungs and skeleton were ignored). These phantoms represented children with ages of 0 (newborn), one, five, ten, and fifteen years of age. These early designs were assumed to have outer dimensions that represented the average height, surface area, and body mass of a child of the particular age. These phantoms became known as the "similitude phantoms" because of their resemblance to children. This approach had its limitations because children are generally not just "little adults." However, these phantoms were the first developed to answer a real need in the nuclear medicine community [22].

In 1969, Snyder and his colleagues reported the first heterogeneous phantom that became known as the "MIRD-5 Phantom," a name derived from the Medical Internal Radiation Dosimetry (MIRD) Committee of the Society of Nuclear Medicine which adopted the phantom [23]. This phantom was composed of a skeleton, a pair of lungs, and the remainder (soft tissue). The representation of internal organs in this mathematical phantom was crude, as the simple equations captured only the most general description of the position and geometry of each organ. The original model was intended to represent a healthy "average" adult male, the Reference Man, as defined by the International Commission on Radiological Protection (ICRP) from an extensive review of medical and other scientific literature on the European and North American populations [246]. The Reference Man was a 20- to 30-year-old Caucasian, 70 kg in weight and 170 cm in height (the height was later changed to 174 cm). In 1978, Snyder et al. published an elaborative set of specific absorbed fractions using an improved version of their

heterogeneous phantom which contained more than 20 organs and more detailed anatomical features [24].

The limitations associated with the approach of applying a set of scaling factors to the adult phantom to create age-dependent similitude phantoms were clear. Significant efforts were undertaken at ORNL during the mid-1970s to develop individual pediatric phantoms based upon a careful review of the existing literature for each particular age. This effort produced the next generation of mathematical phantoms that, although they appeared to be modeled after the adult, were designed independently. Three "individual phantoms" were designed by Hwang et al [25]. This set consisted of the newborn, the one-year, and five-year-old models. A separate effort was undertaken by Jones et al [25] for the 15 years old, and Deus and Poston [26] undertook the design of a 10 years old after the other four designs were complete. The development of the 10 years old was significantly different from those for the other four ages. In fact, this design was intended to point the way to the next generation of more realistic phantoms . Even though the design was completed and used for a limited number of dose calculations, it was not popular because of the very complex geometry and other approaches to the development of phantoms were followed.

12.3.2 Evolution of Stylized Phantoms

Building upon previous work, Cristy reported the development of a new series of stylized phantoms in 1980 and then with Eckerman in 1987 in ORNL/TM-8381 [27, 28]. This series or "family" of phantoms consisted of an adult male, a newborn, and individuals of ages 1, 5, 10, and 15 (also representing an adult female with additional anatomical features). Each phantom is composed of three tissue types with distinct densities: bone, soft tissue, and lung. They were analytically defined in three principal geometric sections as illustrated in Fig. 12.1—an elliptical cylinder representing the arms, torso, and hips; a truncated elliptical cone representing the legs and feet; and an elliptical cylinder representing the head and neck.

In 1995, Stabin and his colleagues at ORNL adapted the adult female phantom in this family to represent a pregnant woman at the end of each trimester of pregnancy [248]. This set of three stylized pregnant female phantoms was used for various internal nuclear medicine applications. Since the 1980s, a number of revised MIRD-5 phantoms were reported which incrementally improved upon the original Fisher-Snyder and Cristy-Eckerman phantoms using the same stylized modeling techniques; however, they are not explicitly listed in Table 1 (i.e., Bouchet et al. on a revised head and brain model [29]. With the availability of general-purpose Monte Carlo codes and affordable computers in the 1980s, this latest series of phantoms, referred to as the "Cristy-Eckerman Phantoms," were quickly adopted by many users for a wide variety of internal dosimetry applications. Later, this set of phantoms was also used for external and internal dosimetry studies [30, 31].

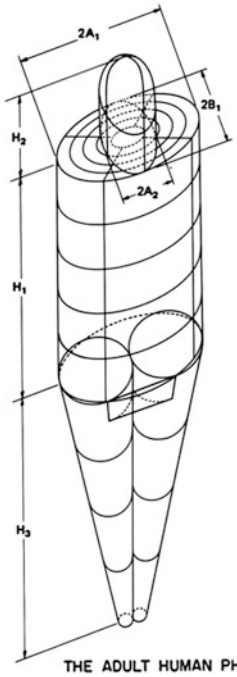

ORNL-DWG. 74-9373

PHANTOM DIMENSIONS AND DOSE REGIONS

Age (yr)	Weight (kg)	H_1 (cm)	H_2 (cm)	H_3 (cm)	A_1 (cm)	B_1 (cm)	A_2 (cm)
0	3.148	23	13	16	5.5	5	4.5
1	9.112	33	16	28.8	8	7	6.5
5	18.12	45	20	46	11	7.5	6.5
10	30.57	54	22	64	14	8	6.5
15	53.95	65	23	78	18	9	7
Adult	69.88	70	24	80	20	10	7

Fig. 12.1 Stylized phantoms

In parallel with the efforts at ORNL by Cristy and Eckerman to revise the MIRD-5 Phantom, Kramer et al. from the GSF, Germany used the anatomical descriptions of the hermaphrodite MIRD-5 phantom to develop a pair of gender-specific adult phantoms known as the ADAM and EVA for external dosimetry studies [32]. The EVA phantom was derived by shrinking all relevant volumes of the MIRD-5 phantom with the total whole-body mass ratio of 0.83 that was revealed from the analysis of ICRP reference organ masses. Then, the female organ masses were modified to create space for neighboring organs. Finally, sex-specific organ such as testes, ovaries, uterus, and breasts were introduced into the appropriate phantom to yield ADAM and EVA, respectively. The chin was introduced by removing a section of the neck to create a more realistic external irradiation geometry for the thyroid. The female breasts were represented by two ellipsoid sections attached to the trunk of EVA. There are a number of minor anatomical differences, such as breast sizes, from those reported by Cristy and Eckerman [28, 32].

The stylized modeling technique was also adopted by one group for medical applications. The mathematical cardiac-torso (MCAT) phantom, which includes the major thoracic structures and organs, was developed by a research group led by Tsui (currently with Johns Hopkins University) at the University of North Carolina for use in nuclear medicine imaging research, specifically single-photon emission computed tomography (SPECT) and positron emission tomography (PET) [33–35].

The same group later developed the first NURBS-based motion-simulating phantom.

The Computational Anatomical Man (CAM) phantom developed by Billings and Yucker in 1973 for the National Aeronautics and Space Administration (NASA) demonstrated a very different and aggressive approach in stylized modeling because the phantom reportedly consisted of 1,100 unique geometric surfaces and 2,450 solid regions [36]. According to the authors, internal body geometries such as organs, voids, bones, and bone marrow were explicitly modeled using CSG modeling techniques. A computer program called CAMERA was also developed for performing analyses with the CAM phantom. The authors state that "extremely detailed geometrical model of the human anatomy, the most detailed yet prepared, has been developed for use in investigations dealing with exposure of astronauts to the natural space radiation environment. The model is equally applicable to investigations dealing with exposure of humans to radiation associated with nuclear weapon and nuclear power system environments as well as medical applications such as radiotherapy and radiography [36]. Indeed the surface geometry was so detailed that one may wonder how this was possible in the 1970s with much less capable computers. Unfortunately, the CAM phantom was never adopted for applications outside the aerospace industry and very little information about the work was accessible by the phantom research community (Tom Jordan, a contracted phantom developer and user, recently released some CAM phantom images at http://cmpwg.ans.org/phantoms.html).

In the early 1990s, it was clear that the research community no longer favored stylized phantom modeling methods. However, several groups continued to develop stylized phantoms for particular methods. Two groups developed computational phantoms of an embryo and fetus for space radiation dosimetry [249] and an adult representing the Korean population [37]. A group at the Nagoya Institute of Technology developed two new stylized phantoms for a 9-month Japanese infants in 2008 [38]. Researchers at the Key Laboratory of Particle & Radiation Imaging in Bejing created a new mathematical phantom named the Chinese mathematical phantom (CMP) in 2008 based on values obtained from the Reference Asian Man and the Chinese Reference Man [39]. A new MIRD phantom based on reference data for the standard Korean male was developed at the Catholic University of Pusan, Bugok [40]. The phantom was used to model a patient implanted with Iridium-192 for brachytherapy of prostate cancer. Bento et al. [41] at the Nuclear and Technological Institute (ITN) of Portugal developed a new mathematical phantom to simulate the reference male BOMAB phantom. The phantom was used to simulate the detection of internal sources of radiation with a whole-body counter (WBC). A series of four mathematical phantoms were developed at the Bhaba Atomic Research Centre to simulate the calibration of whole-body monitoring systems for internal radionuclide contamination using BOMAB phantoms [42].

For 40 years since the first anthropomorphic phantom was reported, these anatomically simplified phantoms have been used as the *de facto* "standard" representations of the ICRP "Reference Man" methodology which is based on "population-average" 50th

percentile anatomical parameters [246, 247]. Applications of stylized phantoms have eventually included many aspects of radiation protection, radionuclide therapy, and medical imaging [43]. In addition, national and international bodies have adopted organ dose estimates derived from these stylized phantoms in guidelines and regulations related to industrial and medical uses of ionizing radiation.

Although stylized phantoms made it possible to carry out Monte Carlo computations during times when computers were much less powerful, the original developers recognized the obvious shortcomings. Human anatomy is too complex to be realistically modeled with a limited set of surface equations. Many anatomical details in these models were compromised that sometimes led to inaccurate results. For example, when such phantoms were applied to nuclear medicine procedures where precise dosimetry is necessary, the calculated average organ and marrow doses did not produced strong correlations with observed marrow toxicity. Most nuclear medicine physicians consequently tend to administer lower-than-optimal amounts of radioactivity to avoid toxicity. For CT dose reporting, all existing commercial software systems are based on the stylized patient models that are known to cause very large errors for low-energy *X*-rays [44]. Similar stylized models have also been used to derive dose–response relationships for Japanese atomic bomb survivors and for medical patients in epidemiological studies. In the external-beam radiotherapy community, an early stylized homogenous phantom was used by the Radiation Epidemiology Branch of the National Cancer Institute (NCI) for nearly 30 years in studies related to organ doses of therapeutically irradiated patients [45]. By the 1980s, a few groups of researchers began to seek new ways to develop anatomically realistic phantoms.

12.3.3 Second-Generation Voxel Phantoms (from late 1980 to Early 2000s)

The development of anatomically realistic models was desirable but impossible until early 1980s when powerful computer and tomographic imaging technologies became available. With the advent of CT and MR imaging techniques, researchers could for the first time visualize the internal structures of the body in three dimensions (3D) and store the images in versatile digital formats. These advantages brought about the exciting and prolific era of the so-called voxel or tomographic phantoms . Xu [5] summarizes a total of 84 phantoms that were constructed from three types of tomographic images: CT and MR images from live subjects, as well as cross sectional photographs of cadavers. In two earlier review articles, the number of voxel phantoms was reported to be 21 by Caon [10] and 38 by Zaidi and Xu [11]. The increase in phantom number reported by Xu [5] was due to a more exhaustive literature search, recent developments, and the inclusion of phantoms developed for use solely in non-ionizing radiation applications.

In terms of solid geometry modeling techniques, a voxel—one of the basic CSG primitives—is simply a 3D representation of a pixel; however, compared with the medical applications such as radiation treatment planning, the task of developing reference human phantoms presented some unique and intractable challenges: (1) to construct a whole-body phantom, image slices should ideally cover the entire body—a process not normally carried out in routine medical examinations because of *X*-ray exposures or the lengthy time required for MR procedures; (2) a large amount of internal organs/tissues must be identified and segmented for organ dose calculations, whereas, in radiotherapy, only the tumor volume and adjacent regions are routinely outlined; (3) the image data size of a whole-body model, especially when high-resolution images are used, can be potentially too great for a computer to handle; and (4) a standardized patient phantom is often used to study diverse radiation types such as photons, electrons, neutrons, and protons, thus requiring considerable Monte Carlo simulation capabilities.

In terms of the developmental process, voxel phantoms are fundamentally different from the stylized ones. A tomographic image data set is composed of many slices, each displaying a 2-dimensional (2D) pixel map of the anatomy. The 3D volume of a voxel is measured by multiplying the pixel size by the thickness of an image slice. Unlike stylized phantoms, which are based on quadric surface equations, a voxel phantom contains a huge number of tiny cubes grouped to represent various anatomical structures. However, both quadric surface equations and voxels (cuboids) belong to the same class of CGS geometries

The creation of a tomographic phantom involves four general steps: (1) acquire a set of tomographic images (e.g., CT, MR, or anatomical photography) that cover the entire volume of the body; (2) identify organs or tissues of interest (e.g., lungs, liver, skin) from the original image slice by assigning every pixel with an identification number; (3) specify the density (e.g., soft tissue, hard bone, air) and chemical composition of organs or tissues; and (4) register the segmented image slices into a 3D volume that can be used for 3D visualization (for checking anatomical structures) and for Monte Carlo calculations. Figure 12.2 illustrates

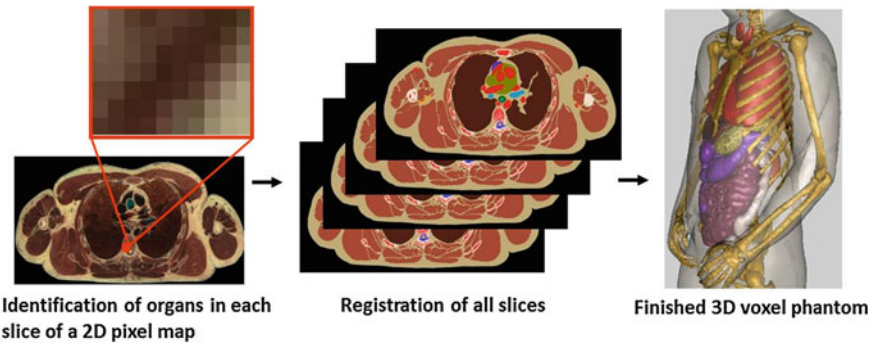

Fig. 12.2 Steps to create a voxel phantom illustrated using the Visible Human cadaver image data set [46]

these steps reported by Xu et al. [46] using the National Library of Medicine's Visible Human image data set.

The earliest effort to create image-based phantoms for radiation protection dosimetry is believed to have been reported by the late Professor S. Julian Gibbs of Vanderbilt University [47–49]. In these pioneering studies, Gibbs and her co-workers explored the use of 2D *X*-ray images as the basis to form an anatomically realistic model of the patient. They used this information in Monte Carlo calculations to assess the doses received by patients who underwent from medical and dental radiological procedures.

Zankl and her colleagues at GSF—National Research Center for Environment and Health in Germany (Now known as HZM—the German Research Center for Environmental Health) decided in the late 1980s to use CT imaging on healthy volunteers to develop what eventually became a family of 12 voxel phantoms: BABY, CHILD, DONNA, FRANK, HELGA, IRENE, GOLEM, GODWIN, VISIBLE HUMAN, LAURA, KLARA, and KATJA [50, 51], Petoussi-Henss 2002, [52–55]. The adult male phantoms were developed first, followed by the adult female, pediatric, and pregnant woman phantoms. The GOLEM and LAURA phantoms have recently undergone significant revision, to yield the REGINA and REX phantoms, which were released to the public as the ICRP Reference Computational Phantoms [56, 57]. Several processes were considered at the time when this set of reference phantoms were developed: (1) CT image data sets of individuals close to the Reference Man and Reference Woman (height and weight) were needed, (2) the data sets were segmented, (3) the body heights were adjusted to reference values by scaling the voxels, (4) the skeletal masses were adjusted to the reference values, and (5) individual organs were adjusted to reference values by adding and subtracting voxels.

In 1994, Zubal et al. [58] from Yale University published a head-torso model named VoxelMan, which was developed from CT images. The original phantom was used for optimizing nuclear medicine imaging. Improvements to the original phantom were made with an MRI scan data of a human brain. Users who are allowed to freely download the original data by using the Internet commonly refer to this phantom as the "Zubal phantom." Two early users later revised the original data to report what are known as the MANTISSUE3-6 and VOXTISS8 phantoms by attaching arms and legs in two different positions to the original torso phantom [59, 60]. Adopting this publically available data, Kramer et al. from Brazil developed an adult male phantom named MAX (Male Adult voXel) in 2003 [61] and later an adult female phantom named FAX in 2004 [62], both adjusted in accordance with ICRP-89 reference body heights and organ masses. Kramer et al. revised the skeletons (cortical bone, spongiosa, medullary yellow bone marrow, and cartilage) of MAX and FAX in 2006 to improve their compatibility with the latest ICRP-103 recommendations. These revised phantoms are known as MAX06 and FAX06. The work by Kramer et al. is one of the earliest efforts to create ICRP-89 compatible voxel phantoms.

In 1996, Dimbylow from the National Radiological Protection Board (NRPB) (now known as the Health Protection Agency) in the United Kingdom reported the

development of an adult male phantom known as NORMAN from MR images [4]. NORMAN, which has a body height similar to the ICRP Reference Man, was first used by Dimbylow in a finite-element simulation code to determine the specific energy absorption rate from exposures to non-ionizing electromagnetic fields [63]. In 1997, his colleague Jones adopted NORMAN to estimate organ doses from external and internal photon sources [64]. In 2005, Dimbylow developed an adult female phantom, NAOMI, also from MRI scans [65, 66]. The phantom was rescaled to a height of 1.63 m and a mass of 60 kg, the dimensions of the ICRP Reference Woman. However, to date, the NAOMI phantom has been used only in non-ionizing radiation calculations. In 2005, a revised version of the NORMAN phantom, called NORMAN-5, was created by Ferrari & Gualdrini from ENEA-ION Istituto di Radioprotezione in Italy to derive external photon dose data [67]. One year later, Dimbylow merged the NAOMI with the stylized fetal phantoms developed by Chen to create a series of hybrid phantoms for pregnant women [68]. The process of adjusting two types of geometrical information was reported to be cumbersome.

In 1999, Caon et al. from Flinders University in Australia reported a torso phantom named ADELAIDE created from CT images of a 14-year-old girl [69, 70]. This phantom was interesting because, for some time, it was the only set of data for a teenage girl, and their studies provided CT dose estimates for this patient group. Caon later summarized his and other researchers' experience on voxel phantoms [10].

Realizing the need for additional phantoms representing children of various ages, Bolch and colleagues from the University of Florida (UF) developed a series of pediatric voxel phantoms that appeared between 2002 and 2006, representing children with ages ranging from newborn to 15 years old [71–73]. This approach was later extended to two groups (Groups A and B) of phantoms. Group A is composed of male and female voxel phantoms of a newborn, 1, 5, 10, and 15 years old for whom the phantom stature, total weight, and individual organ masses are targeted to within 1 % of ICRP Publication 89 reference values. Group B phantoms are constructed by scaling the Group A phantoms up and down to yield phantom at each 1-year-age interval, from newborn to 15 years old. The intent of the UF pediatric series was to provide a reference library of phantoms that could be matched to individual patients for age-specific organ dose assessment.

The VIP-Man voxel phantom was reported in 2000 by Xu and two of his students at Rensselaer Polytechnic Institute (RPI) in the United States [46]. VIP-Man was the first phantom that was based on cross-sectional color photographic images of a cadaver. The original photographs were of a 39-year-old male which were made available through the National Library of Medicine's famous Visible Human Project (VHP). VIP-Man is unique because the digitally captured color transversal photos a 0.33 × 0.33 mm pixel resolution, which was the best resolution at the time, and each photograph was taken after the removal (by shaving) of each successive 1-mm layer by a cryomacrotome [46]. The VIP-Man phantom consists of more than 3.7 billion voxels, and the original images were segmented to yield more than 1,400 organs and tissues, although only approximately 80 organs

and tissues were ultimately adopted for radiation dosimetry purposes. With ultra-fine and color images, attempts were made to segment and label a number of small and radiosensitive tissues including the stomach mucosa, skin, and red bone marrow. The finalized VIP-Man phantom had a heavy body mass of 103 kg, which served as an interesting variation from the ICRP reference value. The VIP-Man was used for a large number of studies in health and medical physics. Later, this group extended the 3D phantom into 4D using the NURBS technique. Several other groups also used the VHP images, but they primarily considered the CT data set without the arms. In 2004, Shi and Xu from RPI also reported the pregnant woman phantom, which was developed from rare partial-body CT images of an eight-month pregnant patient [74]. As of May 15, 2012, this paper on VIP-Man phantom by Xu et al. [46] had been cited 266 times and, according to Google Scholar, making it the most cited paper in "computational dosimetry phantoms."

Two Japanese groups reported their independent efforts to develop voxel phantoms since 2001. Saito et al. [75] from the Japanese Atomic Energy Research Institute (JAERI) developed an adult male model named Otoko (the first Asian phantom) and an adult female phantom named Onago. More recently, Saito et al. has developed the JM, JM2, and JF phantoms which have a refined vertical slice thickness [76–78]. These phantoms were used mainly for radiation dosimetry applications in Japan. The work of Saito et al. was influenced by earlier projects at the GSF. The other group, Nagaoka et al., from the National Institute of Information and Communications Technology (NIICT) in Japan reported an adult male model, named TARO, and an adult female model, named HANAKO, developed from MR images for radiofrequency electromagnetic-field studies [79]. Later, Nagaoka et al. would use a free-form deformation (FFD) to change the exterior features of the adult male phantom to develop Deformed Children phantoms of 3, 5 and 7 years old [78]. The authors reported that it was difficult to develop these phantoms with the FFD algorithm and the internal organs are not adjusted to age-dependent values. The Otoko phantom was recently used in a study to calculate dose conversion coefficients for the Japanese population [80].

Several Korean phantoms have been developed by researchers at Hanyang University in Korea from various image sources: Korean Man (KORMAN), Korean Typical MAN-1 (KTMAN-1), Korean Typical Man-2 (KTMAN-2), High-Definition Reference Korean (HDRK), and Korean WOMAN (KORWOMAN). The HDRK phantom was based on sectioned color photographs of an adult male cadaver that has high image resolution [81, 82]. The early work on these phantoms was carried out by the two Lee brothers, who moved in the early 2000s to the University of Florida, where they gradually published work on the Korean phantoms and also made important contributions to the NURBS-based phantoms. Kim spent several years in the US to complete his PhD. from Texas A&M University and then to serve as a research professor at RPI before returning to Hanyan University as a faculty member in the early 2000s. Their separate involvements in the area of voxel phantom development clearly originated from their experiences in the US. The KTMAN-2 phantoms have been used by Lee et al. [83] to measure the effects of selective collimation in cephalography.

Kim et al. [40] from the Korea Atomic Energy Institute have developed a series of voxel phantoms of different body shapes in order to calculate counting efficiencies for whole-body counters. The phantoms are meant to replace a physical BOMAB phantom, which will not yield proper results for the counting efficiencies in some patients due to differences in body shape, such as from obesity.

Three voxel phantoms representing an adult Chinese male have been reported since 2007: CNMAN produced from color photographs of a cadaver by the China Institute for Radiation Protection [85], VCH produced from a different set of cadaver color photographs by the Huazhong University of Science and Technology [86–88], and CVP produced from MR images by Tsinghua University [89, 51]. The Chinese government undertook the Chinese version of the Visible Human Project that resulted in multiple cadaver image data sets, some with slice thickness as fine as 0.2 mm. The lead developer of the CNMAN phantom, B Zhang, served as a research associate at RPI in 2007–2008. Another new Chinese phantom was developed by Li et al. [89] at the Key Laboratory of Particle and Radiation Imaging in Beijing. The phantom was named the Chinese voxel phantom (CVP) and was used to determine conversion coefficients for the Chinese populace. The phantom was produced from MR images of a young Chinese male and was segmented into 23 different tissues and organs.

Researchers at the French National Institute of Health and Medical Research (INSERM) reported a series of virtual whole-body patient models (WBPM) from CT images [90]. The phantoms accommodate different radiotherapy treatment positions, genders, and age groups. Alzier et al. developed a software tool to take patient data and adjust the phantom's anatomy in order to match the patient's anatomy.

In 2009, the ICRP released its Publication 110 which describes the development and intended use of the so-called ICRP computational phantoms of the Reference Male and Reference Female [56]. This pair of phantoms is based on medical image data of real people, yet is consistent with the data given in Publication 89 [247] on the reference anatomical and physiological parameters for both male and female subjects. The reference phantoms are constructed after modifying the voxel models (Golem and Laura) of two individuals whose body height and mass resembled the reference data. The organ masses of both models were adjusted to the ICRP data on the adult Reference Male and Reference Female, without compromising their anatomical realism. ICRP-110 is big step forward in standardization. However, the techniques used to develop such voxel phantoms were quickly out favor and were replaced by newer techniques.

A voxel phantom named NUDEL (NUmerical moDEL) was developed by Ferrari [91] for use in radiation protection. The phantom was constructed from CT data of the plastic AMOS (Anthropomorphic MOdel for dosimetric Studies) phantom. Dose calculations for several types of nuclide exposure were run in MCNPX code and were compared to values obtained from other voxel phantoms.

Patni et al. [92] of the Bhabha Atomic Research Centre in India published dose conversion coefficients obtained from the ICRP adult voxel phantoms. The study

adapted the phantoms for use in the Monte Carlo code FLUKA and calculated dose conversion coefficients for 9 different organs.

A radiological accident that occurred in South America in 2009 prompted the construction of a personalized voxel phantom to numerically calculate the dose the victim received. Courageot et al. [93] of the Institute for Radiological Protection and Nuclear Safety (IRSN) converted CT scans into a voxel phantom using the Simulation of External Source Accident with Medical Images (SESAME) tool. The dose distribution was calculated using MCNPX code and was used in the treatment of the victim. Courageot et al. [94] reported the Simulation of External Source Accident with Medical Images (SESAME) tool that allows the use of NURBS to model a victim's morphology and posture.

Tung et al. [95] from the Chang Gung University of Taiwan developed a voxel phantom of the Reference Taiwanese Adult. CT images from thirty Taiwanese adults were analyzed by hand and in the software environment 3D-Doctor and compared to reference values to construct the phantom.

Project members of MATSIM (MATROSHKA Simulation) at the Austrian Institute of Technology coordinated research to numerically simulate the effects of irradiation under reference radiation fields in outer space [96]. They created a two-part voxel phantom using the FLUKA Monte Carlo code and CT images from a physical RANDO phantom. The voxel phantom was split into the MATSIM torso and head. The results of the simulations were within one standard deviation of experimental values.

ORNL has not been actively involved in the development of voxel phantoms, although Eckerman was instrumental in the work at GSF related to the ICRP reference computational phantoms and a number of voxel phantom projects at several universities in the US. The only reported effort from ORNL was that of Akkurt et al. [97] on a hybrid of voxel and stylized geometries.

In 2011, the University of Florida (UF) published the results of a study on electron dosimetry using the UF adult male hybrid phantom [250]. Monoenergetic electron emissions, ranging in energy from 10-keV to 10-MeV, were simulated with particular interest on the active bone marrow and total shallow marrow. The skeletal tissues were imposed through whole-body CT images at 1-mm resolution. The results of the study were found to be compatible with the averaged skeletal values of the absorbed fraction given in ICRP 110, but incompatible with the internal dosimetry software used currently.

Recently, a team of scientists from Iran and Japan collaborated to develop a race-specified voxelized organ, specifically a Japanese male liver [98]. The purpose of this development was to have race-specific organ modeling for nuclear medicine and internal dosimetry purposes. The liver was constructed using the digital Zubal phantom and 35 CT scan images for male individuals of Japanese descent. The detailed process for this development included using a point-drift maximum likelihood alignment algorithm. The technique used allowed for the retainment of anatomical realism and provides nuclear medicine dosimetry with statistical parameters.

12.3.4 BREP Phantoms from 2000s to Present

Ten groups reported a total of 183 BREP-based phantoms. Segars's PhD. thesis at the University of North Carolina was the first publication that systematically described the NURBS-based modeling techniques [99]. The cardiac-torso (NCAT) phantom was developed from the Visible Human CT image data set and the 3D anatomy was later extended into the 4th dimension to model cardiac and respiratory motions. The beating heart model of the 4D NCAT was based on 4D tagged MRI data from a real patient. The 4D NCAT phantom offers a vast improvement over the stylized MCAT phantom , with more realistic models of the anatomy and the cardiac system, and the respiratory motions. The 4D NCAT has gained a widespread use particularly in nuclear medicine imaging research for evaluating and improving myocardial SPECT imaging. The conceptual design of the NCAT phantom also served as basis for the development of a 4D digital mouse phantom named MOBY [100, 101]. Segars et al. [102] released an update to the NCAT phantom in the form of a 4D NURBS-based cardiac phantom. The cardiac phantom was constructed from a series of tagged MRI images in the SURFdriver program. The cardiac phantom performs normal cardiac motion in simulations, but Segars released an application that can modify the heart's motion to account for some defects in the same study. The 4D extended cardiac-torso (XCAT) phantom family was recently developed as the next version of the 4D NCAT. It includes more detailed and realistic anatomy and physiology, suitable for use in higher-resolution imaging applications. The XCAT phantom family includes whole-body male and female anatomies based on the high-resolution Visible Male and Female anatomical data sets [103]. In addition to the basic anatomy, the cardiac and respiratory motions were also updated in the XCAT phantom. The series includes 47 phantoms based on of the XCAT phantom. The XCAT phantom was mapped to patient CT data to produce the series. Segars ran simulations of PET, SPECT, and CT to demonstrate the applicability of the phantoms. The NCAT and XCAT phantoms have been used by several research groups to simulate radiation dose from radiography [104, 105] and radiotherapy [237, 106]. A research group constructed a version of the XCAT heart to enhance the range of cardiac disorders that can be studied using the phantom [107]. Tward et al. [108] from John Hopkins University developed a series of pediatric phantoms from a base adult XCAT phantom. They used a MATLAB-based implementation of large deformation diffeomorphic metric mapping (LDDMM) to adjust the XCAT phantom to match pediatric reference data. The implementation used multi-channel LDDMM to treat each organ as a separate image unified by a common background. An algorithm to modify the XCAT phantom was developed and used to generate 24 male pediatric patients with 8 organs each.

In 2005, the research group led by Xu at RPI used the VIP-Man phantom to simulate respiratory motions by adopting the gated respiratory motion data of the NCAT phantom [251]. The 4D VIP-Man Chest phantom was used to study external-beam treatment planning for a lung cancer patient [233]. The group later

decided to apply the BREP techniques to a more challenging problem and, in 2007, reported the development of a series of phantoms representing a pregnant woman and her fetus at the end of 3-, 6-, and 9-month gestations [109]. These phantoms, referred to as the RPI pregnant females, were defined by polygonal meshes which were derived from separate anatomical information of a non-pregnant female, a 7-month pregnant woman CT data set, and a mesh model of the fetus. The organ volumes were adjusted in the mesh format using a commercial software package. The paper by Xu et al. was rated one of the 10 best papers in 2007 by Physics in Medicine and Biology. Continuing their triangular mesh approach, this group reported in 2008 the development of a pair of adult male and female phantoms, the so-called RPI Adult Male and Female [110, 111, 112]. This pair of adult phantoms was carefully adjusted to match the ICRP-89 reference values for more than 70 organs and 45 bones (including cortical bone, spongiosa, and cavities) as well as muscles. Several software algorithms were systematically developed to automate the deformation and organ overlap detection that were based entirely on about 126 sets of triangle meshes. The RPI Adult Male and Female phantoms are mesh-based BREP phantoms [112]. As an application, the female phantom was recently used to create phantoms of female workers with different breast sizes for the purpose of studying the effect of this parameter on the lung counting of internally deposited radionuclides [110]. The mesh models had to be converted to voxels to work with Monte Carlo codes that only handle CSG shapes. In a second application, Ding et al. [113] modified the RPI Adult Male and Female phantoms and produced 10 obese phantoms for the purpose of optimizing image quality and dose in obese patients. The initial study used the obese phantoms in dose calculations, and it was found that calculated dose for obese patients differed significantly from the dose calculated for normal weight phantoms. Taranenko and Xu [225] used the RPI-P phantom series to calculate conversion coefficients for fetuses from whole-body irradiation with monoenergetic proton beams. The simulation was run in MCNPX for 12 different source energies ranging from 100 MeV to 100 GeV, and for 6 different configurations. Gu et al. [114] used the RPI Pregnant Female phantoms to run dose calculations for multi-detector CT (MDCT) scans. The MDCT scanner and the phantoms were implemented in MCNPX code. The dose profiles showed that there was little risk to the patient or the fetus from the MDCT scans.

In 2007 and 2008, the UF group led by Bolch reported their work on the so-called "hybrid" male and female phantoms of newborn and 15-year-old patients [115, 116]. They created the BREP phantom series, called UFH-NURBS phantoms using the following steps. First, they segmented patient-specific CT image data from which they then generated polygonal meshes. These meshes were then converted to the NURBS format using commercial software. In this last process, they extracted several contours from the polygonal meshes and then generated the NURBS surfaces by a software tool called "lofting." It was then in the NURBS geometrical domain they carried out organ adjustment to match the ICRP-89 reference. Therefore, their phantoms are in fact NURBS-based BREP phantoms, like those developed by Segars et al. [99]. In the final step, the NURBS-

based phantoms were voxelized so that they could be implemented in Monte Carlo calculations. However, in order to voxelize the smooth NURBS models, they transferred the NURBS surfaces back the polygonal meshes. The paper by Lee et al. [51] was also rated one of the 10 best papers in 2007 by Physics in Medicine and Biology. In 2011, Maynard et al. [117] from the UF produced a family of NURBS-based fetal phantoms. The phantoms were based on CT and MR images from fetal specimens of various ages between 10 and 30 weeks and were modified to conform to reference values. Tissues and organs were segmented using the modeling software 3D-Doctor and turned into polygon mesh surfaces. The models were then imported into Rhinoceros 3D to incorporate NURBS surfaces and correctly orient the models. The UF phantoms family has seen wide use. The UF hybrid adult male phantom was used in a study by Johnson et al. [118] to calculate the effects of patient size on dose conversion coefficients. A model of electron dosimetry on infants based on the UF hybrid newborn phantom and an earlier developed skeleton tissue model [119] was released by Pafundi et al. [120] from the University of Florida. Hough et al. [121 released a model for skeletal-based electron dosimetry in the ICRP reference male. CT scans of a cadaver were implemented in Rhinoceros 3D to modify the UF hybrid male reference phantom to include segmented skeletal tissue. Dimbylow et al. [122] published a study that used the University of Florida's newborn NURBS-based voxel phantom to calculate SAR for exposure to electromagnetic fields in the 20-MHz to 6-GHz region. Bahadori et al. [123] from the University of Florida released a publication studying dose estimates from space radiation on astronauts. They modeled the astronauts by adapting the UF family of hybrid phantoms to the 5th, 50th, and 95th percentiles for 40-year-old American males and 40-year-old Japanese females.

In 2008, the Vanderbilt group led by Stabin, in collaboration with Segars from Duke University, reported a "family" of adult and pediatric phantoms by adapting the NURBS-based NCAT adult male and female phantoms [124, 125]. ICRP-89 reference body and organ values were used to adjust NURBS surfaces. The authors state several advantages of this approach: (1) NURBS-based phantoms can be developed much more quickly than working with voxels and manually segmenting individual patient image data sets; (2) The phantoms have a higher level of internal consistency; and (3) The phantoms are complete from head to toe, thus avoiding the problem of missing organs in some of the medical images. It is noted that the groups at RPI, UF, and Vanderbilt (and Duke) developed these BREP phantoms as part of the joint Virtual Patients Project funded by the National Cancer Institute as well as other individual projects.

Cassola et al. (2010) at the Federal University of Pernambuco (UFPE) have constructed two phantoms based on polygon mesh surfaces. The phantoms, FASH (Female Adult meSH) and MASH (Male Adult meSH), were constructed using software, including Blender, ImageJ, Binvox, and MakeHuman. The researchers based their phantoms on anatomical models and atlases and showed that whole-body CT scans are unnecessary for phantom design. The organ masses were based on the values recommended for the male and female reference adult in report 89 from the ICRP. Cassola compared FASH and MASH to the RPI-AF and RPI-AM phantoms

and noted significant differences in anatomy. The UFPE group [238] made a series of calculations on the FASH and MASH phantoms. Large differences were observed compared to calculations done on the RPI-AM and RPI -AF mesh phantoms.

In 2010, four phantoms collectively named The Virtual Family were developed for electromagnetic exposure calculations by Christ et al. [126] at the Foundation for Research on Information Technologies in Society (IT'IS). The Virtual Family consists of a 34-year-old adult male, 26-year-old adult female, 11-year-old girl, and a 6-year-old boy. MR images from volunteers were analyzed and segmented into 80 different tissues and organs using the imaging processing software iSEG. The boundaries between the tissues and organs were then remodeled using the software tool Amira. The Virtual Family is a part of the larger Virtual Population project at IT'IS. The Virtual Population project has developed 6 additional anatomical models using the same methods that were used with the Virtual Family [127]. The additional models consist of the Virtual Classroom, a series of four child models, and two individually developed models: an obese 37-year-old male model, and an aged 84-year-old male model.

Cassola et al. [177] continued the work on the FASH and MASH phantoms and published a library of 18 phantoms in 2011. The phantoms were adjusted based on reference values for the 10th, 50th, and 90th height and mass percentiles for Caucasian members of each gender. The reference values were obtained from the PeopleSize software package, which obtained the values from over 100 publications in North America, Asia, Australia, and Europe. In 2011, the group published 5- and 10-year-old pediatric phantoms based on the same methodology that created FASH and MASH [128]. The phantoms were developed with polygon mesh surfaces in the modeling programs Blender and MakeHuman and were edited in the programs DIP (Digital Imaging Processing) and QtVoxel. The researchers used ICRP data for the 5- and 10-year-old reference children. They did not use medical images to construct the phantoms and instead relied on anatomical atlases and modeling software.

The group at IRSN developed a series of female torso phantoms in the Rhinoceros-3D modeling environment [183]. A base thoracic torso phantom was produced from mesh surfaces and NURBS and was based on the reference data from the ICRP adult female reference computational phantom. A series of 34 phantoms of differing girth, cup size, breast tissue composition, and internal organ volumes were created from the base phantom. They used the phantoms to ascertain the morphological dependence of counting efficiency curves from in vivo lung monitoring of workers [129]. In 2011, they released a thoracic male phantom and a mesh equivalent to the physical Livermore phantom for the purposes of simulating in vivo measurements [129]. The phantoms were modeled with mesh and NURBS geometries. Data from CT and MRI scans were analyzed in Isogray to delineate organs. The data were then imported to Rhinoceros 3D, where it was assembled into the two phantoms. Simulations of the two phantoms yielded comparable data to those done with voxel phantoms. The phantoms will be the basis for a new library of phantoms in a future study.

A separate project at the IRSN produced a library of 25 whole-body male phantoms in 2011 [130]. The phantoms were produced from data in the CAESAR

database, a compilation of male and female 3D models constructed from full-body optical imaging. A total of 22 male Caucasian optical models were used as the basis for the phantoms . The phantom's organs were constructed from ICRP reference data and added to the optical models. The phantoms possess a total of 109 segmented organs. The phantoms occupy a range of different body types, organ masses, and organ volumes.

Current permutations of hybrid phantoms must be voxelized so that they may be used in Monte Carlo dose calculations. Voxelizing a hybrid phantom reintroduces the majority of the limitations of the voxel phantoms. Researchers at Hanyang University in Korea have converted the voxel phantom VKH-Man into a polygon surface phantom using 3D-Doctor and directly implemented the phantom into Geant4 in order to circumvent this limitation [131]. Calculations on their new phantom, PSRK-Man (Polygon Surface Reference Korean Man) has been compared to the HDRK-Man phantom, which was also based on VKH-Man. The PSRK-Man phantom has overcome many of the limitations of a voxel phantom; however, the calculation speed for the phantom is 70–150 times slower than for its voxel counterpart HDRK-Man.

12.4 Applications of Computational Phantoms at RPI

Computational phantoms have been used extensive at RPI for diverse health physics and medical physics applications, including external photon beams from 10 keV to 10 MeV [132, 133], external electron beams [134, 135], external neutron beam in low energies (10^{-9} –20 MeV) and in high energy (20–10,000 MeV) [134, 136], external proton beams [137], photon dose to the red bone marrow [174], internal electron dosimetry [138, 139], SPECT and PET brain imaging [140], *X*-ray radiographs [141], *X*-ray image quality ROC/AUC analysis [142], interventional cardiological examinations [143], adjoint Monte Carlo algorithm for external-beam prostate radiation treatment planning [231], non-target organ doses from proton radiation treatments [145], respiration management in IGRT [233], imaging doses in IGRT [44], kV CBCT and MDCT [146], and time-resolved proton range telescope [147]. More information can be found at the website for Rensselaer Radiation Dosimetry and Measurement Group (http://rrmdg.rpi.edu).

12.5 Monte Carlo Methods and Computer Codes

There are a few comprehensive reviews or introductory articles about the Monte Carlo methods for applications in health physics and medical physics [148–150]. Several public-domain and popular Monte Carlo code systems include MCNP (X-5 Monte Carlo Team 2003), MCNPX [151], EGS [152], Geant4 [6, 7, 153], PENELOPE [154–156], and Fluka [157, 158].

12.6 Non-ionizing Radiation Applications

People who have been interested in non-ionizing radiation applications form a different group of voxel phantom developers. Most of this work was neglected in the previous review articles by Caon [10] and by Zaidi and Xu [11]. Interestingly, the phantoms used for studies of temperature rise in the human body from the interactions of radiofrequency energy were constructed through nearly identical steps and some of these phantoms, such as the NORMAN phantom, have been used for both ionizing and non-ionizing radiation applications. However, the majority of voxel phantoms were developed with only one application in mind. Some phantoms have been used for non-ionizing applications: the Visible Man from the VHP color photographs by the Brooks Air Force (Mason et al. 2000), [159], the DAM adult male phantom from MR images by a group in Italy [160], the SILVY 30-week pregnant woman phantom from hybrid CT (originally obtained by RPI) and MR images by the Graz University of Technology, Austria [161, 162], the MEET Man from VHP color photographs by University of Karsrule, Germany [163, 164], and the anatomically based model from MR images by University of Utah [165]. The redundancy in developing voxel phantoms from similar image sets such as the VHP is obvious.

Findlay and Dimbylow [166] from the Health Protection Agency in the UK published a study of the specific absorption rate (SAR) for exposure to electromagnetic fields using the NORMAN phantom. Findlay and Dimbylow [167] continued their work on SAR measurements and conducted a study of SAR in children due to Wi-Fi. He rescaled the sitting posture NORMAN phantom so that it matched ICRP reference values for a 10-year-old child. The effects of electromagnetic fields from Wi-Fi devices operating at 2.4 and 5 GHz were modeled using a FDTD method.

Uusitupa et al. (2010) published a study measuring SAR in the 300- to 5000-MHz region utilizing 15 voxel phantoms, including NORMAN, the Japan Male/Female, the VHP Male, and the VF series. The simulations were run with FDTD code on a HP supercluster at the Helsinki University of Technology in Finland. The study modeled the effects of different postures, human body models, and incoming direction of the electromagnetic field.

A series of 9 phantoms representing a pregnant female in each gestational month developed by a group from the University of Houston and the US. Food Drug Administration (FDA) for studying the effects of radiofrequencies emitted from various electronic devices [168]. These phantoms only include a limited number of organs such as the body, placenta, embryonic fluid, bladder, bone, fetus, and the uterus. They used patient-specific MR images and CAD software to model the organ shapes.

12.7 Discussion and Conclusion

Computational phantoms have come a remarkably long way. Mathematical formulations of organs and tissues of the body used in the dosimetry of internally distributed radionuclides existed as early as the 1940s, although the first anthropomorphic phantom was not reported until the 1960s. In the 1970s and 1980s, the sophistication of these stylized phantoms was increased significantly. This evolution began with the specification of a single organ mass, followed by the use of simple shapes to simulate organs or the entire body of an adult human. The desire to model the entire body of a "Reference Man" and to specify the location, shape, volume, and mass of organs in the body as realistically as possible has remained the same to this day. The climax for stylized phantoms was reached in the 1980s when the gender- and age-specific family phantoms were systematically documented and widely adopted for various studies in internal and external radiation dosimetry, as well as in medical imaging and radiotherapy. By that time, Monte Carlo codes and personal computers had become accessible to a large number of researchers. The research on stylized human models carried out at ORNL up to the 1980s played an essential role in the history of computational phantoms. The sex-specific adult phantoms at GSF in the early 1980s were revisions of the MIRD-5 phantom originally developed at ORNL. Major extensions in the 1990s, on the pregnant women and brain/head models, were also closely tied to the earlier work at ORNL. The direct involvement of ORNL's scientists in the SNM's MIRD Committee facilitated the necessary standardization process. It is clear that close collaborations between leading developers were a key factor contributing to the success of these first-generation computational phantoms. Not all phantoms of this generation enjoyed the same recognition in the history. In fact, a few phantoms such as the CAM have been practically unknown by the mainstream radiation protection dosimetry community. The late 1980s would go into history as the beginning of an exciting new era of voxel phantoms. Collaboration in the information age would soon require new approaches, and as the history would show, no single developer was to dominate the new research agenda as ORNL once did.

The shift from stylized phantoms to voxel phantoms in the late 1980s was motivated by the desire to improve upon anatomical realism. The advent of modern computers and medical imaging fueled the research efforts by many researchers. For a long period of time in the 1990s and early 2000s, however, it was unclear to the research community what roles voxel phantoms would play. If voxel phantoms were to replace stylized phantoms, how much improvement in dose estimates should be expected? There were strong indications already that the approach of developing and applying the voxel phantoms was not perfect. For example, the of original images into organs and tissues required a very laborious and tedious manual process (there is only a limited number of organs such as the skeleton which can be processed automatically and semi-automatically), often taking months or years to complete. The earlier phantoms developed at GSF had relatively poor image slice thickness (from 4 to 8 mm), thus inevitably

compromising the anatomical accuracy. Even today, there is no consensus as to what constitutes a true segmentation because the process often involves some level of user-specific assumption about the anatomy during the image analysis. Certain organs such as the GI tract have poor image contrast, and the segmentation is nearly impossible in CT without enhancement. A typical image data set at more than 2 mm × 2 mm pixel resolution is not fine enough to delineate many small radiosensitive organs. As a result, the skin of most existing voxel phantoms is defined artificially as the outermost layer of voxels. The segmentation of the red bone marrow is also challenging. Consequently, its dose is nearly always calculated empirically because it is not easy to model it directly in the phantom. When the developers of the VIP-Man phantoms reported that the red bone marrow was segmented from color pixels of 0.33 × 0.33 mm resolution, the work was scrutinized by others partially due to the lack of consensus about the segmentation process. The lack of standardized procedures contributed to the current situation that although many phantoms and dosimetry data are reported, the accuracy may be impossible to evaluate.

Original voxel phantoms were realistic in depicting the anatomy, but they are person specific. The anatomical differences between two equally realistic voxel phantoms surprised many developers who were used to the idea that a radiation protection phantom must represent the average population. Realizing that there would be likely only one set of such "reference" phantoms, many developers later rushed to revise the original voxel phantoms by adjusting the organ sizes in the original image data to match with the ICRP recommended anatomical data. Others mixed anatomical sources from different subjects. In doing so, these phantoms lost the anatomical realism, which was the original motivation to abandon the stylized phantoms.

The history of computational phantom development has shown that it is the need for application, not the need for policy-making, which determines the course of technological advancement.

To date, the history of phantom development has been centered on the "Reference Man" paradigm which mandates a computational phantom to match approximately the 50th percentile values in terms of body height and weight for a specific gender and age group. Given the anatomical specificity in any voxel phantom, the Reference Man concept works against the original wish to improve the dose estimate in a population of workers who are obviously different from the anatomy depicted by the one voxel phantom. In contrast, the BREP phantoms may have demonstrated the feasibility to develop new-generation phantoms that represent a much broader range of individuals in terms of body height and weight, as well as organ topology. These features were impossible even 10 years ago, but the technology and collective experience of the research community seems to support that idea that we should and can move beyond the "Reference Man" paradigm.

Xu et al. [46] predicted that the advantages afforded by both the BREP type of surface geometries and anatomically realistic voxels would be eventually combined: "For the purposes of setting radiation protection standards, it may be possible to eventually bridge these two types of models, leading to a new generation

of hybrid 'standard' model(s) that will be acceptable to the radiation protection community. Such a new generation of models for radiation protection should be realistic enough to accurately represent major radiosensitive tissues and organs, and flexible enough to represent different populations by scaling. Computers are going to be so powerful that very complex models can be handled without a problem." Impressively, the BREP phantoms were realized in only several years later.

Looking forward, in the next 10 years, advances in computational phantom research will be mostly driven by the power of new-generation Monte Carlo code and associated applications. There will be, of course, important dosimetry needs that should and can be addresses in the near future: (1) a fundamental change in the Reference-Man-based paradigm, (2) physics-based methods for deformation modeling, (3) posture-specific phantoms using motion capture, (4) phantoms and associated methods that report dose uncertainties, (5) multi-scale phantoms (whole-body phantom to eye phantom) (6) direct Monte Carlo simulations with advanced geometries such as NURBS and meshes, (7) near "real-time" Monte Carlo dose calculation using graphics processing units (GPUs) and other accelerators, (8) Increasingly person-specific whole-body computational phantoms, and (9) virtual-reality enabled computational phantom for treatment planning and training. The 60-year history shows that coordinated and cooperative efforts among radiological engineers, computer scientists, biologists, and clinicians are the key to the success of future research endeavors in computational phantoms.

Acknowledgments Helpful discussions in the past decade with many colleagues, especially K Eckerman, W Bolch, M Stabin, A Brill, WP Segars, B Tsui, H Paganetti, IG Zubal, M Zankl, N Petoussi-Henss, R Kramer, Q Liu, J Li, CH Kim, and K Sato through the Consortium of Computation Human Phantoms (CCHP). This review article is based on several chapters of the "Handbook of Anatomical Models for Radiation Dosimetry" published in 2009. M Pinkert and Ashley Rhodes, undergraduate students at RPI, helped compile the recent literature information. Research at RPI, which is highlighted in this article, involved the following former PhD students: Bozkurt et al. [134, 132, 236], Winslow et al. [169, 144, 239] Bednarz (2008), [240–242], Han et al. [147], Ding et al. [113, 243]. These research projects at RPI were supported by the following grants: National Science Foundation (BES-9875532), National Library of Medicine (R03LM007964, R01LM009362, and R01LM009362-03S1), National Cancer Institute (R01CA116743 and R42CA115122), National Institute of Biomedical Imaging and Bioengineering (R42EB010404), and National Institute of Standards and Technology (70NANB9H9198).

References

1. Attix, F. H. (1986). *Introduction to radiological physics and radiation dosimetry* (Vol. 14). London: Wiley.
2. Hubbell, J. H. (1969). Photon cross sections, attenuation coefficients and energy absorption coefficients from 10 keV to 100 GeV. *NSRDS-NBS* 29.
3. Storm, L., & Israel, H. (1970). Photon cross sections from 1 keV to 100 MeV for elements Z=1 to Z=100. *Atomic Data and Nuclear Data Tables, 7*, 565–681.
4. Dimbylow, P. J. (1996). The development of realistic voxel phantoms for electromagnetic field dosimetry. In *Proceedings Workshop on Voxel Phantom Development*, Chilton, UK.

5. Xu, X. G. (2009). Chapter 1. Computational phantoms for radiation dosimetry: A 40-year history of evolution. In *Handbook of anatomical models for radiation dosimetry*. Taylor & Francis, 2009.
6. Agostinelli, S., et al. (2003). Geant4 a simulation toolkit. *Nuclear instruments and methods in physics research section A, 506*, 250–303.
7. Geant4 Team. (2013). Geant4 user's guide for application developers http://geant4.web.cern.ch/geant4/G4UsersDocuments/UsersGuides/ForApplicationDeveloper/html, Last Accessed Oct 2013.
8. Leyton, M. (2001). *A generative theory of shape*. Berlin: Springer.
9. Stroud, I. (2006). Boundary representation modeling techniques. London: Springer. ISBN: 978-1-84628-312-3.
10. Caon, M. (2004). Voxel-based computational models of real human anatomy: A review. *Radiation and Environmental Biophysics, 42*, 229–235.
11. Zaidi, H., & Xu, X. G. (2007). Computational anthropomorphic models of the human anatomy: The path to realistic Monte Carlo modeling in radiological sciences. *Annual Review of Biomedical Engineering, 9*, 471–500.
12. Marinelli, L. D. (1942). Dosage determination with radioactive isotopes. *American Journal of Roentgenology, 47*, 210.
13. ICRP. (1959). Report of committee II on permissible dose for internal radiation. Oxford,UK: Pergamon Press.
14. Loevinger, R., Japha, E. M., & Brownell, G. L. (1965a). Discrete radioisotope sources. In Hine G. J. & Brownell G. L. (Eds.) *Radiation dosimetry*. New York: Academic Press.
15. Loevinger, R., Hiolt, J. G., & Hine, G. J. (1965b). Internally administered radionuclides. In Hine G. J. & Brownell G. L. (Eds.) *Radiation dosimetry*. New York: Academic Press.
16. Loevinger, R. (1969). Distributed radionuclide sources. In Attix F. H., & Tochilin (Eds.) *Radiation dosimetry* (2nd ed., Vol. 3). New York: Academic Press
17. Marinelli, L. D., Quimby, E. H., & Hine, G. J. (1948). Dosage determination with radioactive isotopes II. Practical considerations in therapy and protection. *American Journal of Roentgenology, 59*, 260.
18. Quimby, E. H. (1970). The development of radiation dosimetry in nuclear medicine. *Medical Radionuclides: Radiation Dose and Effects*, AEC Symposium Series 20.
19. Fisher, H. L. J., & Snyder, W. S. (1966). Variation of dose delivered by 137Cs as a function of body size from infancy to adulthood. *ORNL*-4007.
20. Fisher, H. L. J., & Snyder, W. S. (1967). Distribution of dose in the body from a source of gamma rays distributed uniformly in an organ. *ORNL*-4168.
21. Snyder, W. S. (1968). *Variation of dose in man from exposure to a point source of gamma rays of Congres International sur la Radioprotection dans l'Utilisation Industrielle des Radioelements* (pp. 7–11), Paris, 13–15 Decembre 1965. Paris, Service Centra de Protection Contre les Rayonnements Io.
22. Kereiakes, J. G., Seltzer, R. A., Blackburn, B., & Saenger, E. L. (1965). Radionuclide doses to infants and children: A plea for a standard child. *Health Physics, 11*, 999–1004.
23. Snyder, W. S., Fisher, H. L., Ford, M. R., & Warner, G. G. (1969). Estimates of absorbed fractions for monoenergetic photon sources uniformly distributed in various organs of a heterogeneous phantom. *Journal of Nuclear Medicine, 3*(Suppl), 7–52.
24. Snyder, W. S., Ford, M. R., & Warner, G. G. (1978). Estimates of specific absorbed fractions for monoenergetic photon sources uniformly distributed in various organs of a heterogeneous phantom. *MIRD Pamphlet*, *5*, Revised.
25. Jones, R. M. et al. (1976) The development and use of a fifteen-year-old equivalent mathematical phantom for internal dose calculations. *ORNL/TM*-5278.
26. Deus, S. F., & Poston, J. W. (1976). The development of a mathematical phantom representing a 10-year-old for use in internal dose calculations. In *Proceedings of the Symposium on Radiopharmaceutical Dosimetry HEW Publication (FDA) 76-8044*, Oak Ridge, TN.

27. Cristy, M. (1980). *Mathematical phantoms representing children of various ages for use in estimates of internal dose.*
28. Cristy, M. & Eckerman, K.F. (1987). Specific absorbed fractions of energy at various ages from internal photon sources I: Methods, *ORNL/TM*-8381/V1.
29. Bouchet, L. G., Bolch, W. E., Weber, D. A., Atkins, H. L., & Poston, J. W. (1999). MIRD Pamphlet No. 15: Radionuclide S values in a revised dosimetric model of the adult head and brain. Medical internal radiation dose. *Journal of Nuclear Medicine, 40*, 62S–101S.
30. Markovic, V. M., Krstic, D., & Nikezic, D. (2009). Gamma and beta doses in human organs due to radon progeny in human lung. *Radiation Protection Dosimetry, 135*, 197–202.
31. Takahashi, F., Shigemori, Y., & Seki, A. (2009). Accurate dose assessment system for an exposed person utilising radiation transport calculation codes in emergency response to a radiological accident. *Radiation Protection Dosimetry, 133*, 35–43.
32. Kramer, R. et al. (1982). The calculation of dose from external photon exposures using reference human phantoms and Monte Carlo methods: Part I. The male (ADAM) and female (EVA) adult mathematical phantoms. *GSF-Report* S-885.
33. Pretorius, P. H., Xia, W., King, M. A., Tsui, B. M., Pan, T. S., & Villegas, B. J. (1997). Evaluation of right and left ventricular volume and ejection fraction using a mathematical cardiac torso phantom. *Journal of nuclear medicine official publication Society of Nuclear Medicine, 38*, 1528–1535.
34. Tsui, B. M. W., Zhao, X. D., Gregoriou, G. K., Lalush, D. S., Frey, E. C., Johnston, R. E., et al. (1994). Quantitative cardiac SPECT reconstruction with reduced image degradation due to patient anatomy. *Nuclear Science, IEEE Transactions on, 41*, 2838–2844.
35. Tsui, B. M., Terry, J. A., & Gullberg, G. T. (1993). Evaluation of cardiac cone-beam single photon emission computed tomography using observer performance experiments and receiver operating characteristic analysis. *Investigative Radiology, 28*, 1101–1112.
36. Billings, M. P., & Yucker, W. R. (1973). *The Computerized Anatomical Man CAM Model, NASA CR-134043*. Washington, DC: Government Printing Office.
37. Park, S., Lee, J. K., & Lee, C. (2006). Development of a Korean adult male computational phantom for internal dosimetry calculation. *Radiation Protection Dosimetry, 121*, 257–264.
38. Hirata, A., Ito, N., Osamu, Fujiwara, Nagaoka, T., & Watanabe, S. (2008). Conservative estimation of whole-body-averaged SARs in infants with a homogeneous and simple-shaped phantom in the GHz region. *Physics in Medicine & Biology, 53*, 7215–7223.
39. Qiu, R., Li, J., Zhang, Z., Wu, Z., Zeng, Z., & Fan, J. (2008). Photon SAF calculation based on the Chinese mathematical phantom and comparison with the ORNL phantoms. *Health Physics, 95*, 716–724.
40. Kim, J. S., Ha, W. H., Jeong, J. H., Cho, K.-W., & Ki, Lee Jai. (2010). Use of photographic images to construct voxel phantoms for use in whole-body counting. *Radiation Protection Dosimetry, 138*, 119–122.
41. Bento, J., Barros, S., Teles, P., Neves, M., Gonçalves, I., Corisco, J., & Vaz, P. (2011). Monte carlo simulation of the movement and detection efficiency of a whole-body counting system using a BOMAB phantom. *Radiation Protection Dosimetry,* 1–11.
42. Bhati, S., Patni, H. K., Ghare, V. P., Singh, I. S., & Nadar, M. Y. (2011). Monte carlo calculations for efficiency calibration of a whole-body monitor using BOMAB phantoms of different sizes. *Radiation Protection Dosimetry,* 1–6.
43. ICRU. (1992). *Phantoms and computational models in therapy, diagnosis and protection*. *ICRU Report 48*. Bethesda: International Commission on Radiation Units and Measurements.
44. Gu, J. W., Bednarz, B., Xu, X. G., & Jiang, S. (2008). Assessment of patient organ doses and effective doses using the VIP-Man adult male phantom for selected cone-beam CT imaging procedures during image guided radiation therapy. *Radiation Protection Dosimetry, 131*, 431–443.
45. Stovall, M., Smith, S. A., & Rosenstein, M. (1988). Tissue doses from radiotherapy of cancer of the uterine cervix. *Medical Physics, 16*, 726–733.

46. Xu, X. G., Chao, T. C., & Bozkurt, A. (2000). VIP-Man: An image-based whole-body adult male model constructed from color photographs of the visible human project for multi-particle Monte Carlo calculations. *Health Physics, 78*, 476–486.
47. Gibbs, S., & Pujol, J. (1982). A Monte Carlo method for patient dosimetry from diagnostic x-ray. *Dentomaxillofac Radiol, 11*, 25.
48. Gibbs, S. J., Pujol, A., Chen, T. S., Malcolm, A. W., & James, A. E. (1984). Patient risk from interproximal radiography. *Oral Surgery, Oral Medicine, Oral Pathology, 58*, 347–354.
49. Gibbs, S. et al. (1987). Radiation doses to sensitive organs from intraoral dental radiography. *Dentomaxillofac Radiol, 16*.
50. Fill, U. A., Zankl, M., Petoussi-Henss, N., Siebert, M., & Regulla, D. (2004). Adult female voxel models of different stature and photon conversion coefficients for radiation protection. *Health Physics, 86*, 253–272.
51. Zeng, Z., et al. (2007). Dose assessment for space radiation using a proton differential dose spectrum. *Journal of Tsinghua University (Science and Technology), 46*, 374.
52. Williams, G., Zankl, M., Abmayr, W., Veit, R., & Drexler, G. (1986). The calculation of dose from external photon exposures using reference and realistic human phantoms and Monte Carlo methods. *Physics in Medicine & Biology, 31*, 449–452.
53. Zankl, M., Veit, R., Williams, G., Schneider, K., Fendel, H., Petoussi, N., et al. (1988). The construction of computer tomographic phantoms and their application in radiology and radiation protection. *Radiation and Environmental Biophysics, 27*, 153–164.
54. Zanki, M., Fill, U., Petoussi-Henss, N., & Regulla, D. (2002). Organ dose conversion coefficients for external photon irradiation of male and female voxel models. *Physics in Medicine & Biology, 47*, 2367–2385.
55. Zankl, M. et al. (2005). GSF male and female adult voxel models representing ICRP Reference Man–the present status. In *Proceedings of The Monte Carlo Method: Versatility Unbounded in a Dynamic Computing World*, Chattanooga, TN, American Nuclear Society, A Grange Park, USA.
56. ICRP. (2009). Adult reference computational phantoms. *ICRP publication, 110*. Pergamon Press.Oxford, UK: Pergamon Press.
57. Schlattl, H., Zankl, M., & Petoussi-Henss, N. (2007). Organ dose conversion coefficients for voxel models of the reference male and female from idealized photon exposures. *Physics in Medicine & Biology, 52*, 2123–2145.
58. Zubal, I. G., Harrell, C. R., Smith, E. O., Rattner, Z., Gindi, G., & Hoffer, P. B. (1994). Computerized three-dimensional segmented human anatomy. *Medical Physics, 21*, 299–302.
59. Dawson, T. W., Caputa, K., & Stuchly, M. A. (1997). A comparison of 60 Hz uniform magnetic and electric induction in the human body. *Physics in Medicine & Biology, 42*, 2319–2329.
60. Sjögreen, K., Ljungberg, M., Wingårdh, K., Erlandsson, K., & Strand, S. E. (2001). Registration of emission and transmission whole-body scintillation-camera images. *Journal of Nuclear Medicine, 42*, 1563–1570.
61. Kramer, R., Vieira, J. W., Khoury, H. J., Lima, F. R. A., & Fuelle, D. (2003). All about MAX: A male adult voxel phantom for Monte Carlo calculations in radiation protection dosimetry. *Physics in Medicine & Biology, 48*, 1239–1262.
62. Kramer, R., Khoury, H. J., Vieira, J. W., Loureiro, E. C. M., Lima, V. J. M., Lima, F. R. A., et al. (2004). All about FAX: A Female Adult voXel phantom for Monte Carlo calculation in radiation protection dosimetry. *Physics in Medicine & Biology, 49*, 5203–5216.
63. Dimbylow, P. J. (1997). FDTD calculations of the whole-body averaged SAR in an anatomically realistic voxel model of the human body from 1 MHz to 1 GHz. *Physics in Medicine & Biology, 42*, 479–490.
64. Jones, D. G. (1997). A realistic anthropomorphic phantom for calculating organ doses arising from external photon irradiation. *Radiat Prot Dosimetry, 72*, 21–29.

65. Dimbylow, P. (2005). Development of the female voxel phantom, NAOMI, and its application to calculations of induced current densities and electric fields from applied low frequency magnetic and electric fields. *Physics in Medicine & Biology, 50*, 1047–1070.
66. Dimbylow, P. (2005). Resonance behaviour of whole-body averaged specific energy absorption rate (SAR) in the female voxel model, NAOMI. *Physics in Medicine & Biology, 50*, 4053–4063.
67. Ferrari, P., & Gualdrini, G. (2005). An improved MCNP version of the NORMAN voxel phantom for dosimetry studies. *Physics in Medicine & Biology, 50*, 4299–4316.
68. Dimbylow, P. (2006). Development of pregnant female, hybrid voxel-mathematical models and their application to the dosimetry of applied magnetic and electric fields at 50 Hz. *Physics in Medicine & Biology, 51*, 2383–2394.
69. Caon, M., Bibbo, G., & Pattison, J. (2000). Monte carlo calculated effective dose to teenage girls from computed tomography examinations. *Radiation Protection Dosimetry, 90*, 445–448.
70. Caon, M., Bibbo, G., & Pattison, J. (1999). An EGS4-ready tomographic computational model of a 14-year-old female torso for calculating organ doses from CT examinations. *Physics in Medicine & Biology, 44*, 2213–2225.
71. Lee, C., Nagaoka, T., & LEE, J. K. (2006). Implementation of Japanese male and female tomographic phantoms to multi-particle Monte Carlo code for ionizing radiation dosimetry. *Journal of Nuclear Science and Technology, 43*, 937–945.
72. Nipper, J. C., Williams, J. L., & Bolch, W. E. (2002). Creation of two tomographic voxel models of paediatric patients in the first year of life. *Physics in Medicine & Biology, 47*, 3143–3164.
73. Lee, C., Williams, J. L., Lee, C., & Bolch, W. E. (2005). The UF series of tomographic computational phantoms of pediatric patients. *Medical Physics, 32*, 3537–3548.
74. Shi, C., & Xu, X. G. (2004). Development of a 30-week-pregnant female tomographic model from computed tomography (CT) images for Monte Carlo organ dose calculations. *Medical Physics, 31*, 2491–2497.
75. Saito, K., Wittmann, A., Koga, S., Ida, Y., Kamei, T., Funabiki, J., et al. (2001). Construction of a computed tomographic phantom for a Japanese male adult and dose calculation system. *Radiation and Environmental Biophysics, 40*, 69–75.
76. Sato, K., Noguchi, H., Emoto, Y., Koga, S., & Saito, K. (2007). Japanese adult male voxel phantom constructed on the basis of CT images. *Radiation Protection Dosimetry, 123*, 337–344.
77. Sato, K., Noguchi, H., Endo, A., Emoto, Y., Koga, S., & Saito, K. (2007). Development of a voxel phantom of Japanese adult male in upright posture. *Radiation Protection Dosimetry, 127*, 205–208.
78. Saito, K. et al. (2008). Construction of a voxel phantom based on CT data for a Japanese female adult and its use for calculation of organ doses from external electrons, Japanese. *Journal of Health Physics, 43*(2), 122–130.
79. Nagaoka, T., Watanabe, S., Sakurai, K., Kunieda, E., Watanabe, S., Taki, M., et al. (2004). Development of realistic high-resolution whole-body voxel models of Japanese adult males and females of average height and weight, and application of models to radio-frequency electromagnetic-field dosimetry. *Physics in Medicine & Biology, 49*, 1–15.
80. Takahashi, M., Kinase, S., & Kramer, R. (2011). Evaluation of counting efficiencies of a whole-body counter using Monte Carlo simulation with voxel phantoms. *Radiation Protection Dosimetry, 144*, 407–410.
81. Choi, S. H. et al. (2006). Construction of a high-definition 'Reference Korean' voxel phantom fro organ and tissue radiation dose calculation. In *World Congress on Medical Physics and Biomedical Engineering*, Seoul, Korea
82. Kim, C. H., Choi, S. H., Jeong, J. H., Choonsik, Lee, & Chung, M. S. (2008). HDRK-Man: A whole-body voxel model based on high-resolution color slice images of a Korean adult male cadaver. *Physics in Medicine & Biology, 53*, 4093–4106.

83. Lee, B., Shin, G., Kang, S., Shin, B., Back, I., Park, H., Park, C., Lee, Jeongwoo., Lee, W., Choi, J., Park, R., Kim, Y. (2011). Dose evaluation of selective collimation effect in cephalography by measurement and Monte Carlo simulation. *Radiation Protection Dosimetry*, 1–7.
85. Zhang, B., Ma, J., Liu, L., & Cheng, J. (2007). CNMAN: A Chinese adult male voxel phantom constructed from color photographs of a visible anatomical data set. *Radiation Protection Dosimetry, 124*, 130–136.
86. Zhang, G., Liu, Q., & Luo, Q. (2007). Monte Carlo simulations for external neutron dosimetry based on the visible Chinese human phantom. *Physics in Medicine & Biology, 52*, 7367–7383.
87. Zhang, G., Liu, Q., Zeng, S., & Luo, Q. (2008). Organ dose calculations by Monte Carlo modeling of the updated VCH adult male phantom against idealized external proton exposure. *Physics in Medicine & Biology, 53*, 3697–3722.
88. Zhang, G., Luo, Q., Zeng, S., & Liu, Q. (2008). The development and application of the visible Chinese human model for Monte Carlo dose calculations. *Health Physics, 94*, 118–125.
89. Li, J.L., Qiu, R., Zhang, Z., Liu, L.Y., Zeng, Z., Bi, L., & Li, W.Q. (2009). Organ dose conversion coefficients for external photon irradiation using the Chinese voxel phantom (CVP). *Radiation Protection Dosimetry*, *135*, 33–42.
90. Alziar, I., Bonniaud, G., Couanet, D., Ruaud, J. B., Vicente, C., Giordana, G., et al. (2009). Individual radiation therapy patient whole-body phantoms for peripheral dose evaluations: Method and specific software. *Physics in Medicine & Biology, 54*, N375–N383.
91. Ferrari, P. (2010). Development of an integrated couple of anthropomorphic models for dosimetric studies. *Radiation Protection Dosimetry, 142*, 191–200.
92. Patni, H. K., Nadar, M. Y., Akar, D. K., Bhati, S., & Sarkar, P. K. (2010). Selected organ dose conversion coefficients for external photons calculated using Icrp adult voxel phantoms and Monte Carlo code fluka. *Radiation Protection Dosimetry,* 1–11.
93. Courageot, E., Huet, C., Clairand, I., Bottollier-Depois, J. F., & Gourmelon, P. (2011). Numerical dosimetric reconstruction of a radiological accident in South America in April 2009. *Radiation Protection Dosimetry, 144*, 540–542.
94. Courageot, E., Sayah, R., & Huet, C. (2010). Development of modified voxel phantoms for the numerical dosimetric reconstruction of radiological accidents involving external sources: Implementation in SESAME tool. *Physics in Medicine & Biology, 55*, N231–N241.
95. Tung, C. J., Tsai, S. F., Tsai, H. Y., & Chen, I. J. (2011). Determination of voxel phantom for reference Taiwanese adult from CT image analyses. *Radiation Protection Dosimetry, 146*, 186–190.
96. Beck, P., Zechner, A., Rollet, S., Berger, T., Bergmann, R., Hajek, M., et al. (2011). *MATSIM : Development of a voxel model of the MATROSHKA astronaut dosimetric phantom, 58*, 1921–1926.
97. Akkurt H., Bekar K. B., & Eckerman K. F. (2008). VOXMAT: Phantom model with combination of voxel and mathematical geometry, *53rd Annual Health Physics Society Meeting*, Pittsburgh, PA, July 13–17.
98. Mofrad, F. B., Zoroofi, R. A., Tehrani-Fard, A. A., Akhlahpoor, S., Hori, M., Chen, Y. W., et al. (2010). Statistical construction of a Japanese male liver phantom for internal radionuclide dosimetry. *Radiation Protection Dosimetry, 141*, 140–148.
99. Segars, W. P. (2001). Ph.D thesis, University of North Carolina at Chapel Hill, pp. 243.
100. Segars, W. P., Tsui Benjamin, M. W., Frey Eric, C., Johnson, G. A., & Berr, S. S. (2004). Development of a 4-D digital mouse phantom for molecular imaging research. *Molecular Imaging and Biology MIB the Official Publication of the Academy of Molecular Imaging, 6*, 149–159.
101. Segars, W., & Tsui, B. (2007). 4D MOBY and NCAT phantoms for medical imaging simulation of mice and men. *Society of Nuclear Medicine Annual Meeting Abstracts, 48*, 203.

102. Segars Paul, W., Lalush David, S., Frey Eric, C., Manocha, D., King, Ma., & Tsui Benjamin, M. W. (2009). Improved dynamic cardiac phantom based on 4D NURBS and tagged MRI. *IEEE Transactions on Nuclear Science, 56*, 2728–2738.
103. Segars, W. P., Sturgeon, G. M., Ward, D. J., Ratnanather, J. T., Miller, M. I., & Tsui, B.M. W. (2010). The New XCAT Series of Digital Phantoms for Multi-Modality Imaging. *Journal of the Acoustical Society of America*, 2392–2395.
104. Tabary, J., Marache-Francisco, S., Valette, S., Segars, W.P., & Lartizien, C. (2009). Realistic X-ray CT simulation of the XCAT phantom with SINDBAD. In *2009 IEEE Nuclear Science Symposium Conference Record (NSS/MIC)* (pp. 3980–3983).
105. Niu, X., Yang, Y., Jin, M., Wernick, M. N., & King, Ma. (2010). Regularized Fully 5D Reconstruction of Cardiac Gated Dynamic SPECT Images. *IEEE Transactions on Nuclear Science, 57*, 1085–1095.
106. Peroni, M., Spadea, M. F., Riboldi, M., Baroni, G., Chen, G. T. Y., Sharp, G. C., Medicine, C., & Magna, S. (2009). *Validation of an automatic contour propagation method for lung cancer 4D adaptive radiation therapy*. Boston, MA: Department of Radiation Oncology, Massachusetts General Hospital, 4 Harvard Medical Methods, pp. 1071–1074
107. Veress, A. I., Segars, W. P., Tsui Benjamin, B. M., & Gullberg, G. T. (2011). Incorporation of a left ventricle finite element model defining infarction into the XCAT imaging phantom. *IEEE Transactions on Medical Imaging, 30*, 915–927.
108. Tward, D. J., Ceritoglu, C., Sturgeon, G., Segars, W. P., Miller, M. I., & Ratnanather, J. T. (2011). Generating patient-specific dosimetry phantoms with whole-body diffeomorphic image registration. In *Bioengineering Conference (NEBEC), 2011 IEEE 37th Annual Northeast* (pp. 1–2). IEEE.
109. Xu, X. G., Taranenko, V., Zhang, J., & Shi, C. (2007). A boundary-representation method for designing whole-body radiation dosimetry models: Pregnant females at the ends of three gestational periods–RPI-P3, -P6 and -P9. *Physics in Medicine & Biology, 52*, 7023–7044.
110. Hegenbart, L., Na, Y. H., Zhang, J. Y., Urban, M., & Xu, X. G. (2008). A Monte Carlo study of lung counting efficiency for female workers of different breast sizes using deformable phantoms. *Physics in Medicine & Biology, 53*, 5527–5538.
111. Xu, X. G., Zhang, J. Y., & Na, Y. H. (2008). Preliminary data for mesh-based deformable phantom development: Is it possible to design person-specific phantoms on-demand. *The International Conference on Radiation Shielding-11*.
112. Na, Y. H., Zhang, B., Zhang, J., Caracappa, P. F., & Xu, X. G. (2010). Deformable adult human phantoms for radiation protection dosimetry: Anthropometric data representing size distributions of adult worker populations and software algorithms. *Physics in Medicine & Biology, 55*, 3789–3811.
113. Ding, A., Mille, M. M., Liu, T., Caracappa, P. F., & Xu, X. G. (2012). Extension of RPI-adult male and female computational phantoms to obese patients and a monte carlo study on the effects on CT imaging dose. *Physics in Medicine & Biology, 57*, 2441–2459.
114. Gu, J., Bednarz, B., Caracappa, P. F., & Xu, X. G. (2009). The development, validation and application of a multi-detector CT (MDCT) scanner model for assessing organ doses to the pregnant patient and the fetus using Monte Carlo simulations. *Physics in Medicine & Biology, 54*, 2699–2717.
115. Lee, C., Lodwick, D., Hasenauer, D., Williams, J. L., Lee, C., & Bolch, W. E. (2007). Hybrid computational phantoms of the male and female newborn patient: NURBS-based whole-body models. *Physics in Medicine & Biology, 52*, 3309–3333.
116. Lee, C., Lodwick, D., Williams, J. L., & Bolch, W. E. (2008). Hybrid computational phantoms of the 15-year male and female adolescent: Applications to CT organ dosimetry for patients of variable morphometry. *Medical Physics, 35*, 2366–2382.
117. Maynard, M. R., Geyer, J. W., Aris, J. P., Shifrin, R. Y., & Bolch, W. (2011). The UF family of hybrid phantoms of the developing human fetus for computational radiation dosimetry. *Physics in Medicine & Biology, 56*, 4839–4879.

118. Johnson, P., Choonsik, Lee, Johnson, K., Siragusa, D., & Bolch Wesley, E. (2009). The influence of patient size on dose conversion coefficients: A hybrid phantom study for adult cardiac catheterization. *Physics in Medicine & Biology, 54*, 3613–3629.
119. Pafundi, D., Lee, C., Watchman, C., Bourke, V., Aris, J., Shagina, N., et al. (2009). An image-based skeletal tissue model for the ICRP reference newborn. *Physics in Medicine & Biology, 54*, 4497–4531.
120. Pafundi, D., Rajon, D., Jokisch, D., Lee, Choonsik, & Bolch, W. (2010). An image-based skeletal dosimetry model for the ICRP reference newborn–internal electron sources. *Physics in Medicine & Biology, 55*, 1785–1814.
121. Hough, M., Johnson, P., Rajon, D., Jokisch, D., Lee, C., & Bolch, W. (2011). An image-based skeletal dosimetry model for the ICRP reference adult male–internal electron sources. *Physics in Medicine & Biology, 56*, 2309–2346.
122. Dimbylow, P., Bolch, W., & Lee, C. (2010). SAR calculations from 20 MHz to 6 GHz in the University of Florida newborn voxel phantom and their implications for dosimetry. *Physics in Medicine & Biology, 55*, 1519–1530.
123. Bahadori, A. A., Van Baalen, M., Shavers, M. R., Dodge, C., Semones, E. J., & Bolch Wesley, E. (2011). The effect of anatomical modeling on space radiation dose estimates: A comparison of doses for NASA phantoms and the 5th, 50th, and 95th percentile male and female astronauts. *Physics in Medicine & Biology, 56*, 1671–1694.
124. Stabin, M., Emmons, M. A., Segars, W. P., Fernald, M., & Brill, A. B. (2008). ICRP-89 based adult and pediatric phantom series. *Society of Nuclear Medicine Annual Meeting Abstracts, 49*, 14.
125. Stabin, M. G., Xu, X. G., Emmons, M. A., Segars, W. P., Shi, C., & Fernald, M. J. (2012). RADAR reference adult, pediatric and pregnant female phantom series for internal and external dosimetry. *Journal of Nuclear Medicine, 53*(11), 1807–1813.
126. Christ, A., Kainz, W., Hahn, E. G., Honegger, K., Zefferer, M., Neufeld, E., et al. (2010). The Virtual Family–development of surface-based anatomical models of two adults and two children for dosimetric simulations. *Physics in Medicine & Biology, 55*, N23–N38.
127. IT'IS. (2013). The virtual population: High-resolution anatomical models http://www.itis.ethz.ch/services/anatomical-models/virtual-population/ Last Accessed Dec 2013.
128. de Melo Lima, V. J., Cassola, V. F., Kramer, R., de Oliveira Lira, C. A. B., Khoury, H. J., & Vieira, J. W. (2011). Development of 5- and 10-year-old pediatric phantoms based on polygon mesh surfaces. *Medical Physics, 38*, 4723.
129. Farah, J., Broggio, D., & Franck, D. (2011). Examples of Mesh and NURBS modelling for in vivo lung counting studies. *Radiation Protection Dosimetry, 144*, 344–348.
130. Broggio, D., Beurrier, J., Bremaud, M., Desbrée, a, Farah, J., Huet, C., et al. (2011). Construction of an extended library of adult male 3D models: Rationale and results. *Physics in Medicine & Biology, 56*, 7659–7692.
131. Kim, C. H., Jeong, J. H., Bolch Wesley, E., Cho, K.-W., & Hwang, S. B. (2011). A polygon-surface reference Korean male phantom (PSRK-Man) and its direct implementation in Geant4 Monte Carlo simulation. *Physics in Medicine & Biology, 56*, 3137–3161.
132. Chao, T. C., Bozkurt, A., & Xu, X. G. (2001). Conversion coefficients based on the VIP-Man anatomical model and EGS4-VLSI code for external monoenergetic photons from 10 keV to 10 MeV. *Health Physics, 81*, 163.
133. Chao, T. C., Bozkurt, A., & Xu, X. G. (2003). Correction to Conversion coefficients based on the VIP-Man anatomical model and EGS4-VLSI code for external monoenergetic photons from 10 keV to 10 MeV. *Health Physics, 84*(3), 390.
134. Bozkurt, A., Chao, T. C., & Xu, X. G. (2000). Fluence-to-dose conversion coefficients below 20 MeV based on the VIP-Man anatomical model. *Physics in Medicine & Biology, 45*, 3059.
135. Chao, T. C., Bozkurt, A., & Xu, X. G. (2001). Organ dose conversion coefficients for 0.1–10 MeV electrons calculated for the VIP-MAN tomographic model. *Health Physics, 81*, 203.

136. Bozkurt, A., Chao, T. C., & Xu, X. G. (2001). Fluence-to-dose conversion coefficients based on the VIP-Man anatomical model and MCNPX code for monoenergetic neutrons above 20 MeV. *Health Physics, 81*, 184.
137. Bozkurt, A., & Xu, X. G. (2004). Fluence-to-dose Conversion Coefficients for Monoenergetic Proton Beams Based on the VIP-Man Anatomical Model. *Radiation Protection Dosimetry, 112*(2), 219.
138. Chao, T. C., & Xu, X. G. (2001). Specific absorbed fractions from the image-based VIP-Man body model and EGS4-VLSI Monte Carlo code: Internal electron emitters. *Physics in Medicine & Biology, 46*, 901.
139. Xu, X. G., Chao, T. C., & Bozkurt, A. (2005). Comparison of effective doses from various monoenergetic particles based on the stylised and the VIP-Man tomographic models. *Radiation Protection Dosimetry, 115*, 530.
140. Chao, T. C., & Xu, X. G. (2004). S-values calculated from a tomographic head/brain model for brain imaging. *Physics in Medicine & Biology, 49*, 4971.
141. Winslow, M., Huda, W., Xu, X. G., Chao, T. C., Shi, C. Y., Ogden, K. M., et al. (2004). Use of the VIP-Man Model to Calculate Energy Impacted and Effective Dose for X-ray Examinations. *Health Physics, 86*, 174.
142. Son, I. Y., Winslow, M., Yazici, B., & Xu, X. G. (2006). X-ray imaging optimization using virtual phantoms and computerized observer modelling. *Physics in Medicine & Biology, 51*, 4289.
143. Bozkurt, A., & Bor, D. (2007). Simultaneous determination of equivalent dose to organs and tissues of the patient and of the physician in interventional radiology using the Monte Carlo method. *Physics in Medicine & Biology, 52*, 317.
144. Wang, B., Xu, X. G., Goorley, J. T., & Bozkurt, A. (2005a). The use of MCNP code for an extremely large voxel model VIP-Man. The Monte Carlo method: Versatility unbounded. In A dynamic computing world. American Nuclear Society (ISBN: 0-89448-695-0).
145. Jiang, H., Wang, B., Xu, X. G., Suit, H. D., & Paganetti, H. (2005). Simulation of organ-specific patient effective dose due to secondary neutrons in proton radiation treatment. *Physics in Medicine & Biology, 50*, 4337.
146. Ding, A., Gu, J., Trofimov, A. V., & Xu, X. G. (2010). Monte Carlo calculation of imaging doses from diagnostic multidetector CT and kilovoltage cone-beam CT as part of prostate treatment plans. *Medical Physics, 37*, 6199–6204.
147. Han, B., Xu, X. G., & Chen, G. T. Y. (2011). Proton radiography and fluoroscopy of lung tumors: A Monte Carlo study using patient-specific 4DCT phantoms. *Medical Physics, 38*(4), 1903–1911.
148. Andreo, P. (1991). Monte Carlo techniques in medical radiation physics. *Physics in Medicine & Biology, 36*, 861–920.
149. Raeside, D. E. (1976). Monte Carlo principles and applications. *Physics in Medicine & Biology, 21*, 181–197.
150. Turner, J. E., Wright, H. A., & Hamm, R. N. (1985). A Monte Carlo primer for health physicists. *Health Physics, 48*, 717–733.
151. Pelowitz, D. B. (2005). MCNPX User's Manual Version 2.5.0, *Los Alamos National Laboratory report* LA-CP-05-0369.
152. NRC. (2013). EGSnrc http://irs.inms.nrc.ca/software/egsnrc/ Last Accessed Dec 2013.
153. Allison, J., Amako, K., Apostolakis, J., Araujo, H., Arce Dubois, P., Asai, M., et al. (2006). Geant4 developments and applications. *IEEE Transactions on Nuclear Science, 53*, 270–278.
154. NEA. (2013). Penelope2011, A code system for Monte-Carlo Simulation of Electron and Photon transport http://www.oecd-nea.org/tools/abstract/detail/NEA-1525/ Last Accessed Dec 2013.
155. Salvat, F., Fernández-Varea, J. M., & Sempau, J. (2003). PENELOPE, a code system for Monte Carlo simulation of electron and photon transport. *Simulation, 5*, 253.

156. Badal, A., Kyprianou, I., Banh, D. P., Badano, A., & Josep, Sempau. (2009). penMesh–Monte Carlo radiation transport simulation in a triangle mesh geometry. *IEEE Transactions on Medical Imaging, 28*, 1894–1901.
157. Battistoni, G., Cerutti, F., Fassò, A., Ferrari, A., Muraroi, S., Ranft, J., et al. (2007). The FLUKA code: Description and benchmarking. *Aip Conference Proceedings, 896*, 31–49.
158. Fluka Team. (2013). FLUKA http://www.fluka.org/fluka.php Last Accessed Dec 2013.
159. Wang, B., Xu, X. G., & Kim, C. H. (2004). A Monte Carlo CT model of the rando phantom. *Transactions-American Nuclear Society, 90*, 473.
160. Mazzurana, M., Sandrini, L., Vaccari, A., Malacarne, C., Cristoforetti, L., & Pontalti, R. (2003). A semi-automatic method for developing an anthropomorphic numerical model of dielectric anatomy by MRI. *Physics in Medicine & Biology, 48*, 3157–3170.
161. Cech, R., Leitgeb, N., & Pediaditis, M. (2007). Fetal exposure to low frequency electric and magnetic fields. *Physics in Medicine & Biology, 52*, 879–888.
162. Cech, R., Leitgeb, N., & Pediaditis, M. (2008). Current densities in a pregnant woman model induced by simultaneous ELF electric and magnetic field exposure. *Physics in Medicine & Biology, 53*, 177–186.
163. Doerfel, H., & Heide, B. (2007). Calibration of a phoswich type partial body counter by Monte Carlo simulation of low-energy photon transport. *Radiation Protection Dosimetry, 123*, 464–472.
164. Sachse, F.B. et al. (1997). MEET man—Models for simulation of electromagnetic, elastomechanic and thermic behavior of man. Erstellung und technische Parameter, Institut für Biomedizinische Technik: *Universität Karlsruhe.*
165. Tinniswood, A. D., Furse, C. M., & Gandhi, O. P. (1998). Power deposition in the head and neck of an anatomically based human body model for plane wave exposures. *Physics in Medicine & Biology, 43*, 2361–2378.
166. Findlay, R. P., & Dimbylow, P. J. (2009). Spatial averaging of fields from half-wave dipole antennas and corresponding SAR calculations in the NORMAN human voxel model between 65 MHz and 2 GHz. *Physics in Medicine & Biology, 54*, 2437–2447.
167. Findlay, R. P., & Dimbylow, P. J. (2010). SAR in a child voxel phantom from exposure to wireless computer networks (Wi-Fi). *Physics in Medicine & Biology, 55*, N405–N411.
168. Wu, D., Shamsi, S., Chen, J., & Kainz, W. (2006). Evaluations of specific absorption rate and temperature increase within pregnant female models in magnetic resonance imaging birdcage coils. *IEEE Transactions on Microwave Theory and Techniques, 54*, 4472–4478.
169. Winslow, M., Xu, X. G., & Yazici, B. (2005). Development of a simulator for radiographic image optimization. *Computer Methods and Programs in Biomedicine*, *78*(3), 179–190
170. Alderson, S. W., Lanzl, L. H., Rollins, M., & Spira, J. (1962). An instrumented phantom system for analog computation of treatment plans. *The American journal of roentgenology, radium therapy, and nuclear medicine, 87*, 185–195.
171. Anon. (1975). *Report of the task group on reference man* (Vol. 23). Ottawa: ICRP Publication.
172. Briesmeister, J. F. (2003). MCNP—A general monte carlo N-particle transport code *LAUR031987.*
173. Capello, K., Kedzior, S., & Kramer, G. H. (2012). Voxel phantoms: The new ICRP computational phantoms: how do they compare? *Health Physics, 102*(6), 626–630.
174. Caracappa, P. F., Chao, T. C. E., & Xu, X. G. (2009). A study of predicted bone marrow distribution on calculated marrow dose from external radiation exposures using two sets of image data for the same individual. *Health Physics, 96*, 661–674.
175. Carlo, M. (2010). Extension of the NCAT phantom for the investigation of intra-fraction respiratory motion in IMRT using 4D. *Lung,* 1475.
176. Cassola, V. F. (2010). FASH and MASH: Female and male adult human phantoms based on polygon mesh surfaces: I. Development of the anatomy. *Physics in Medicine & Biology*, *55*(1), 133.

177. Cassola, V. F., Milian, F. M., Kramer, R., de Oliveira Lira, C., & Khoury, H. J. (2011). Standing adult human phantoms based on 10th, 50th and 90th mass and height percentiles of male and female Caucasian populations. *Physics in Medicine & Biology, 56*, 3749–3772.
178. CCHP. (2005). "Tomographic models for radiation protection dosimetry" Session, Monte Carlo 2005 Topical Meeting: The Monte Carlo Method: Versatility Unbounded In A Dynamic Computing World., Chattanooga, TN, USA, April 17–21, 2005.
179. Cheung, A. A., Niu, T., Faber, T. L., Segars, W. P., Zhu, L., & Chen, J. (2010). Simulation of left ventricular dyssynchrony using the XCAT phantom. In *Nuclear Science Symposium Conference Record (NSS/MIC), 2010 IEEE* (pp. 3187–3189).
180. CIRS. (2013). Tissue Simulation and Phantom Technology http://www.cirsinc.com Last Accessed Dec 2013.
181. Coulot, J. (2003). Therapeutic applications of monte carlo calculations in nuclear medicine. *Physics in Medicine & Biology, 48*, 2575.
182. CMPWG. (2013). Phantoms http://cmpwg.ans.org/phantoms/camera.pdf Last Accessed July 2013.
183. Farah, J., Broggio, D., & Franck, D. (2010). Female workers and in vivo lung monitoring: A simple model for morphological dependence of counting efficiency curves. *Physics in Medicine & Biology, 55*, 7377–7395.
184. Ferrari, A., Pelliccioni, M., & Pillon, M. (1997). Fluence to effective dose and effective dose equivalent conversion coefficients for electrons from 5 MeV to 10 GeV. *Radiation Protection Dosimetry, 69*, 97.
185. Furler, M. (2007). *Methods of converting geometry*. In CAD To MCNP Code. M.S. thesis. Rensselaer Polytechnic Institute.
186. Geant4 Team. (2013). Working groups http://geant4.web.cern.ch/geant4/collaboration/working_groups.shtml#wg.Run Last Accessed Dec 2013.
187. Gjonaj, E., Bartsch, M., Clemens, M., Schupp, S., & Weiland, T. (2002). High-resolution human anatomy models for advanced electromagnetic field computations. *IEEE Transactions on Magnetics, 38*, 357–360.
188. Griffith, R., Dean, P., Anderson, A., & Fisher, J. (1978). *Fabrication of a tissue-equivalent torso phantom for intercalibration of in vivo transuranic-nuclide counting facilities*.
189. Gu, J., Dorgu, A., & Xu X. G. (2008). Comparison of main software packages for CT dose reporting. *Review Literature And Arts Of The Americas.*
190. Hwang, J. M. L., Shoup, R. L., & Poston, J. W. (1976). Mathematical description of a newborn human for use in dosimetry calculations *ORNL/TM*-5453.
191. ICRP. (1990). Recommendations of the international commission on radiological protection. *ICRP Publication 60.* Oxford, UK: Pergamon Press.
192. Jin, W., Lim, Y. J., Xu, X. G., Singh, T. P., & De, S. (2005). Improving the visual realism of virtual surgery. *Proceedings of Medicine Meets Virtual Reality* (Vol. 13) Long Beach CA, IOS Press. pp. 227.
193. Jones, A. K., Simon, T. A., Bolch, W. E., Holman, M. M., & Hintenlang, D. E. (2006). Tomographic physical phantom of the newborn child with real-time dosimetry I. Methods and techniques for construction. *Medical Physics, 33*, 3274–3282.
194. Katagiri, M., Hikoji, M., Kitaichi, M., Sawamura, S., & Aoki, Y. (2000). Effective dose and organ doses per unit fluence calculated for monoenergetic 0.1 MeV to 100 MeV electrons by the MIRD-5 phantom. *Radiation Protection Dosimetry, 90*(4), 393.
195. Kim, J. I., Choi, H., Lee, B. I., Lim, Y. K., Kim, C. S., Lee, J. K., et al. (2006). Physical phantom of typical Korean male for radiation protection purpose. *Radiation Protection Dosimetry, 118*, 131–136.
196. Kramer, G. H., Burns, L., & Noel, L. (1991). The BRMD BOMAB phantom family. *Health Physics, 61*, 895–902.
197. Kramer, R. (2010). FASH and MASH: Female and male adult human phantoms based on polygon mesh surfaces: II. Dosimetric calculations. *Physics in medicine & biology*, *55*(1), 163

198. Kramer, R., Khoury, H. J., Vieira, J. W., & Lima, V. J. M. (2006). MAX06 and FAX06: Update of two adult human phantoms for radiation protection dosimetry. *Physics in Medicine & Biology, 51*, 3331–3346.
199. Kyoto Kagaku co., LTD. (2013). Hands-on for Health Care Professionals—Simulators, Training Models, and Phantoms http://www.kyotokagaku.com/ Last Accessed Dec 2013.
200. Lee, C., Lee, C., Williams, J. L., & Bolch, W. E. (2006). Whole-body voxel phantoms of paediatric patients–UF Series B. *Physics in Medicine & Biology, 51*, 4649–4661.
201. Lee, C., Lee, C., Park, S.-H., & Lee, J.-K. (2006). Development of the two Korean adult tomographic computational phantoms for organ dosimetry. *Medical Physics, 33*, 380–390.
202. Lee, C., Lee, J., & Lee, C. (2004). Korean adult male voxel model KORMAN segmented from magnetic resonance images. *Medical Physics, 31*, 1017–1022.
203. Lee, C., & Lee, J. (2005). Reference Korean human models: Past, present, and future, *The Monte Carlo Method: versatility unbounded in a dynamic computing world*, Chattanooga, Tennessee.
204. Liu, X. P., Luo, Y. T., & Tong, L. L. (2005). Development and application of MCNP auto-modeling tool: Mcam 3.0. *Fusion Engineering and Design, 75*, 1275–1279.
205. Marzocchi, O., Breustedt, B., Mostacci, D., Zankl, M., & Urban, M. (2011). Theoretical assessment of whole body counting performances using numerical phantoms of different gender and sizes. *Radiation Protection Dosimetry, 144*, 339–343.
206. Menzel, H.-G., Clement, C., & DeLuca, P. (2009). ICRP Publication 110. Realistic reference phantoms: An ICRP/ICRU joint effort. A report of adult reference computational phantoms. *Ann ICRP, 39*, 1–164.
207. Nagaoka, T., Togashi, T., Saito, K., Takahashi, M., Ito, K., Ueda, T., et al. (2006). An anatomically realistic voxel model of the pregnant woman and numerical dosimetry for a whole-body exposure to RF electromagnetic fields. *International Conference of the IEEE, Engineering in Medicine & Biology Society, 1*, 5463–5467.
208. Nagaoka, T., Kunieda, E., & Watanabe, S. (2008). Proportion-corrected scaled voxel models for Japanese children and their application to the numerical dosimetry of specific absorption rate for frequencies from 30 MHz to 3 GHz. *Physics in Medicine & Biology, 53*, 6695–6711.
209. Nagaoka, T., Togashi, T., Saito, K., Takahashi, M., Ito, K., & Watanabe, S. (2007). An anatomically realistic whole-body pregnant-woman model and specific absorption rates for pregnant-woman exposure to electromagnetic plane waves from 10 MHz to 2 GHz. *Physics in Medicine & Biology, 52*, 6731–6745.
210. NCRP. (1985). *The experimental basis for absorbed-dose calculations in medical uses of radionuclides*, NCRP Report No 83.
211. Niu, X., Yang, Y., & Wernick, M. N. (2011). Temporal regularization in fully 5D reconstruction of cardiac gated dynamic spect images, 1504–7.
212. Petoussi-Henss, N., Zanki, M., Fill, U., & Regulla, D. (2002). The GSF family of voxel phantoms. *Physics in Medicine & Biology, 47*, 89–106.
213. Phantom Laboratory. (2013). RANDO Phantoms http://www.phantomlab.com/rando.html Last Accessed Dec 2013.
214. Qiu, R., Li, J., Zhang, Z., Liu, L., Bi, L., & Ren, L. (2009). Dose conversion coefficients based on the Chinese mathematical phantom and MCNP code for external photon irradiation. *Radiation Protection Dosimetry, 134*, 3–12.
215. Reiher, W., Hammersley, J. M., & Handscomb, D. C. (1966) *Monte Carlo methods*. London: Methuen & Co., New York: Wiley, 1964. VII+178 S., Preis: 25s *Biom Z, 8*, 209–209.
216. Sato, K., Noguchi, H., Emoto, Y., Koga, S., & Saito, K. (2009). Development of a Japanese adult female voxel phantom. *Journal of Nuclear Science and Technology, 46*, 907–913.
217. Segars, W. P., Mahesh, M., Beck, T. J., Frey, E. C., & Tsui, B. M. W. (2008). Realistic CT simulation using the 4D XCAT phantom. *Medical Physics, 35*, 3800.

218. Shypailo, R. J., & Ellis, K. J. (2011). Whole body counter calibration using Monte Carlo modeling with an array of phantom sizes based on national anthropometric reference data. *Physics in Medicine & Biology, 56*, 2979–2997.
219. Smans, K., Tapiovaara, M., Cannie, M., Struelens, L., Vanhavere, F., Smet, M., et al. (2008). Calculation of organ doses in x-ray examinations of premature babies. *Medical Physics, 35*, 556–568.
220. Smith, T. J., Petouissi, N., & Zankl, M. (2000). Comparison of internal radiation doses estimated by MIRD and voxel techniques for a "family" of phantoms. *European Journal of Nuclear Medicine, 27*, 1387.
221. Snyder, W. S., Ford, M. R., Warner, G. G., & Fisher, Jr H. L. (1969). Estimates of Absorbed Fractions for Monoenergetic Photon Sources Uniformly Distributed in Various Organs of a Heterogeneous Phantom. *Journal of Nuclear Medicine*, 10.
222. Stabin, M. G., Sharkey, R. M., & Siegel, J. A. (2011). RADAR commentary: Evolution and current status of dosimetry in nuclear medicine. *Journal of Nuclear Medicine, 52*, 1156–1161.
223. Staton, R. J., Jones, A. K., Lee, C., Hintenlang, D. E., Arreola, M. M., Williams, J. L., et al. (2006). A tomographic physical phantom of the newborn child with real-time dosimetry. II. Scaling factors for calculation of mean organ dose in pediatric radiography. *Medical Physics, 33*, 3283–3289.
224. Takahashi, F., Sato, K., Endo, A., Ono, K., Yoshitake, T., Hasegawa, T., et al. (2011). Waza-Ari: Computational dosimetry system for X-Ray Ct examinations. I. radiation transport calculation for organ and tissue doses evaluation using Jm phantom. *Radiation Protection Dosimetry, 146*, 241–243.
225. Taranenko, V., Xu, X.G. (2009). Foetal dose conversion coefficients for ICRP-compliant pregnant models from idealised proton exposures. *Radiation Protection Dosimetry, 133*, 65–72.
226. Tresser, M. A., & Hintenlang, D. E. (1999). Construction of a newborn dosimetry phantom for measurement of effective dose. *Health Physics, 76*, S190.
227. Uusitupa, T. (2010). SAR variation study from 300 to 5,000 MHz for 15 voxel models including different postures. *Radio Science, 1157*.
228. Valentin, J. (2002). Anatomical and physiological data for use in radiological protection: Reference. *Ann ICRP, 13*, 2347–2350.
229. Wang, J., Fujiwara, O., Watanabe, S., & Yamanaka, Y. (2004). Computation with a parallel FDTD system of human-body effect on electromagnetic absorption for portable telephones. *Microwave Theory and Techniques, IEEE Transactions on, 52*, 53–58.
230. Wang, B., Xu, X. G., Goldstein, M., & Sahoo, N. (2005b). Adjoint Monte Carlo method for prostate external photon beam treatment planning: An application to 3-D patient anatomy. *Physics in Medicine & Biology, 50*, 923.
231. Xu, X. G. (2005). Preliminary development of a 4D anatomical model for Monte Carlo simulations. *Medicine*, 1–10.
232. Zhang, J., Na, Y., & Xu, X. G. (2008c). MO-E-AUD B-05: Development of whole-body phantoms representing an average adult male and female using surface-geometry methods. *Medical Physics, 35*, 2875.
233. Zhang, J., Xu, G. X., Shi, C., & Fuss, M. (2008d). Development of a geometry-based respiratory motion-simulating patient model for radiation treatment dosimetry. *Journal of Applied Clinical Medical Physics, 9*, 2700.
234. Ziriax, J. M., Smith, K. I., Nelson, D. A., Ryan, K. L., Gajsek, P., D'Andrea, J. A., et al. (2000). Effects of frequency, permittivity, and voxel size on predicted specific absorption rate values in biological tissue during electromagnetic-field exposure. *IEEE Transactions on Microwave Theory and Techniques, 48*, 2050–2058.
235. Hammersley, J.M., & Handscomb, D.C. (1964). *Monte carlo methods*. London: Chapman & Hall. ISBN:9780412158704.

236. Shi, C.Y. (2004). Development and application of a tomographic model from CT images forcalculating internal dose to a pregnant woman. *Dissertation*, Rensselaer Polytechnic Institute, Troy, New York.
237. McGurk, R., Seco, J., Riboldi, M., Wolfgang, J., Segars, P., & Paganetti, H. (2010). Extension of the NCAT phantom for the investigation of intra-fraction respiratory motion in IMRT using 4D Monte Carlo. *Physics in Medicine and Biology*, *55*, 1475–1490.
238. Kramer, R. (2010). FASH and MASH: female and male adult human phantoms based on polygon mesh surfaces: II. *Dosimetric calculations*, *163*.
239. Caracappa, P. (2006). Development and evaluation of a new algorithm for determining radiation dose to the red bone marrow. *Dissertation*, New York: Rensselaer Polytechnic Institute, Troy.
240. Zhang, J.Y. (2009). A pair of mesh-based phantoms representing ICRP-89 50th-percentile adult males and females for radiation protection dosimetry using Monte Carlo simulations. *Dissertation*, New York: Rensselaer Polytechnic Institute, Troy.
241. Na, Y.H. (2009). Deformable adult human phantoms for radiation protection dosimetry: methods for adjusting body and organ sizes to match population-based percentile data. *Dissertation*, New York: Rensselaer Polytechnic Institute, Troy.
242. Gu, J.W. (2010). Development of CT scanner models for patient organ dose calculations using Monte Carlo methods. *Dissertation*, New York: Rensselaer Polytechnic Institute, Troy.
243. Mille, M. (2013). A study of shape-dependent partial volume correction in pet imaging using ellipsoidal phantoms fabricated via rapid prototyping. *Dissertation*, New York: Rensselaer Polytechnic Institute, Troy.
244. Eckerman, K.F., Stabin, M.G. (2000). Electron absorbed fractions and dose conversion factors for marrow and bone by skeletal regions. *Health Physics*, *78*, 199–214.
245. Xu, X.G., Eckerman, K.F. (2009). *Computational phantoms for radiation dosimetry: a 40-year history of evolution. Handbook of Anatomical Models for Radiation Dosimetry*. Boca Raton: Taylor & Francis, 1–40.
246. ICRP (1975). Report of the Task Group on Reference Man. *ICRP Publication 23*. Pergamon Press. Oxford, UK:Pergamon Press.
247. ICRP (2002). Basic anatomical and physiological data for use in radiological protection reference values. *ICRP Publication 89*. Oxford, UK: Pergamon Press.
248. Stabin, M.G., Watson, E.E., Cristy, M., Ryman, J.C., Eckerman, K.F., Davis, J.L., Marshall, D., Gehlen, M.K. (1995). *Mathematical models and specific absorbed fractions of photon energy in the nonpregnant adult female and at the end of each trimester of pregnancy ORNL Report ORNL/TM 12907*. Oak Ridge, TN: Oak Ridge National Laboratory.
249. Chen, J. (2004). Mathematical models of the embryo and fetus for use in radiological protection. *Health Physics*, *86*, 285–295.
250. Hough, M., Johnson, P., Rajon, D., Jokisch, D., Lee, C., Bolch, W. (2011). An image-based skeletal dosimetry model for the ICRP reference adult male–internal electron sources. *Physics in Medicine and Biology*, *56*, 2309–2346.
251. Xu, X.G., Shi, C.Y. (2005). *Preliminary development of a 4D anatomical model for Monte Carlo simulations Monte Carlo 2005 Topical Meeting*. Chattanooga, TN: American Nuclear Society, LaGrange Park (IL).